



**HAL**  
open science

## **A multi-technique approach to characterization: the Sant Martí de Tous chert as a prehistoric resource for the NE of the Iberian Peninsula**

Bruno Gómez de Soler, María Soto, Ángel Carrancho, Francesc Gispert-Guirado, Hans Mommsen, Juan Ignacio Morales, Alicia Muñoz del Pozo, Clodoaldo Roldán, Aleix Eixea, M. Gema Chacón, et al.

### ► To cite this version:

Bruno Gómez de Soler, María Soto, Ángel Carrancho, Francesc Gispert-Guirado, Hans Mommsen, et al.. A multi-technique approach to characterization: the Sant Martí de Tous chert as a prehistoric resource for the NE of the Iberian Peninsula. *Archaeological and Anthropological Sciences*, 2023, 15 (6), pp.85. 10.1007/s12520-023-01780-x . hal-04132234

**HAL Id: hal-04132234**

**<https://hal.science/hal-04132234>**

Submitted on 22 Feb 2024

**HAL** is a multi-disciplinary open access archive for the deposit and dissemination of scientific research documents, whether they are published or not. The documents may come from teaching and research institutions in France or abroad, or from public or private research centers.

L'archive ouverte pluridisciplinaire **HAL**, est destinée au dépôt et à la diffusion de documents scientifiques de niveau recherche, publiés ou non, émanant des établissements d'enseignement et de recherche français ou étrangers, des laboratoires publics ou privés.



Distributed under a Creative Commons Attribution - NonCommercial - ShareAlike 4.0 International License



# A multi-technique approach to characterization: the Sant Martí de Tous chert as a prehistoric resource for the NE of the Iberian Peninsula

Bruno Gómez de Soler<sup>1,2</sup> · María Soto<sup>3,4</sup> · Ángel Carrancho<sup>5</sup> · Francesc Gispert-Guirado<sup>6</sup> · Hans Mommsen<sup>7</sup> · Juan Ignacio Morales<sup>1,2</sup> · Alicia Muñoz del Pozo<sup>8,1,2</sup> · Clodoaldo Roldán<sup>9</sup> · Aleix Eixea<sup>10</sup> · M. Gema Chacón<sup>1,2,11</sup> · Miguel Soares-Remiseiro<sup>12</sup> · Josep Vallverdú<sup>1,2</sup>

Received: 8 August 2022 / Accepted: 29 April 2023 / Published online: 24 May 2023  
© The Author(s) 2023

## Abstract

The Sant Genís Formation is located in the NE of the Iberian Peninsula (Catalonia, Spain) and is dated to the Priabonian (upper Eocene), being part of the evaporitic formations of the margin of the Ebro Basin. It is formed by a succession of sandy lutites, occasional limestone layers, marls, and local stratified gypsum and cherts, including the Sant Martí de Tous chert. The Sant Martí de Tous chert type is confirmed by its abundance at specific locations within the territory (NE Iberian Peninsula). This is an important raw material procurement area, as evidenced by the presence of this chert in the main prehistoric sites of the region (e.g., Abric Romaní) and the constant discovery of new sites in the area around the Sant Genís Formation, especially from the Neolithic period onwards (e.g., Cal Sitjo, La Guinardera Nord workshop). All these features, together with the great heterogeneity of the Cenozoic evaporitic cherts, prompted us to carry out a multi-proxy characterization for obtaining a valid criterion by which to identify this chert in the archaeological record. This very heterogeneity hampers the macroscopic characterization of archaeological cherts (e.g., at Abric Romaní), but through petrographic analysis we have been able to identify their origins and, albeit to a lesser extent, their lithostratigraphic unit of provenance within the formation. The complementary mineralogical and geochemical techniques applied in this study show that, although it is difficult to establish an exact origin, through intensive sampling and criteria such as the differential presence of Fe and Ca, some differences among the siliceous varieties within a formation can be detected.

**Keywords** Multi-proxy characterization · Sant Martí de Tous chert · Lithic procurement · Chert territory

✉ Bruno Gómez de Soler  
bgomez@iphes.cat

✉ María Soto  
marial.soto@uam.es

<sup>1</sup> Institut Català de Paleocologia Humana i Evolució Social (IPHES-CERCA), Zona Educacional 4, Campus Sescelades URV (Edifici W3), 43007 Tarragona, Spain

<sup>2</sup> Àrea de Prehistòria, Universitat Rovira i Virgili (URV), Campus Catalunya, Av. Catalunya, 35, 43002 Tarragona, Spain

<sup>3</sup> Madrid Institute for Advanced Study (MIAS), Casa Velázquez, Ciudad Universitaria C/de Paul Guinard, 3 28040, Madrid, Spain - Universidad Autónoma de Madrid, C/ Einstein 13 Pabellón C 1ª Planta, 28049 Madrid, Spain

<sup>4</sup> Universidad Autónoma de Madrid, Departamento de Prehistoria Y Arqueología, Facultad de Filosofía Y Letras, Ciudad Universitaria de Cantoblanco, 28049 Madrid, Spain

<sup>5</sup> Área de Prehistoria, Dpto. Historia, Geografía i Comunicació, Universidad de Burgos, Plaza Misael Bañuelos, S/N, 09001 Burgos, Spain

<sup>6</sup> Servei de Recursos Científics i Tècnics, Universitat Rovira i Virgili, Av. Països Catalans 26, 43007 Tarragona, Catalonia, Spain

<sup>7</sup> Helmholtz-Institut Für Strahlen- Und Kernphysik, Universität Bonn, Nussallee 14 – 16, 53113 Bonn, Germany

<sup>8</sup> Universidad de Zaragoza, Depto. de Ciencias de La Tierra, C/ Pedro Cerbuna 12, 50009 Saragossa, Spain

<sup>9</sup> Instituto de Ciencia de los Materiales (ICMUV), Universitat de València, C/Catedrático José Beltrán, 2, 46980 Paterna, Valencia, Spain

<sup>10</sup> Departament de Prehistòria, Arqueologia i Història Antiga, Universitat de València, Av. Blasco Ibáñez 28, 46010 Valencia, Spain

<sup>11</sup> UMR 7194 - Histoire Naturelle de L'Homme Préhistorique (CNRS/MNHN/UPVD), Musée de L'Homme, 17 Place du Trocadéro, 75116 Paris, France

<sup>12</sup> Interdisciplinary Centre for Archaeology and the Evolution of Human Behaviour, Universidade Do Algarve, Faro, Portugal

## Introduction

The Sant Martí de Tous chert (SMT) was widely exploited as a raw material in prehistoric times due to its quality for knapping and its high abundance within a well-delimited area. Indeed, this area became a key location for raw material procurement and stone-tool configuration. The exploitation of this territory has been documented through the continuous use of this chert type. From the Middle Paleolithic (e.g., Abric Romaní) through the Upper Paleolithic (e.g., Esquerda de les Alzines), the Mesolithic (e.g., Abric Agut, Cal Sitjo), the Neolithic (e.g., Vilars de Tous, Cal Sitjo), and even during modern times, when it was employed for the configuration of gunflints (e.g., La Guinardera Nord) (Clop et al. 2005; Rey-Solé et al. 2014; Gómez de Soler et al. 2020a, 2021).

The SMT chert, an evaporitic lithotype from the Sant Genís Formation (Priabonian, upper Eocene), has been studied in recent years in what is considered a prominent chert outcropping area, concentrated in a small region. The area acted as a territorial organizer through the procurement of lithic raw materials among the prehistoric hunter-gatherers and the first farmers who inhabited the northeastern Iberian Peninsula. Located between inland and coastline, north and south, the area connects different ecotones (transitional space between two ecosystems), suggesting that it served as a strategic transit area. This is evidenced by the high number of sites located in the region from the Upper Pleistocene forward and the exponential increase in occupations from the Neolithic onwards. Relevant examples include the Middle Paleolithic sites of Mediona (Estévez et al. 1993), La Noguera (Sant Quintí de Mediona) (Freixas and Mir 1987) and Teixonerer cave (Moià) (Picin et al. 2020), the archaeological sequences of Cova Gran (Collbató) and Simanya Gran (Sant Llorenç del Munt) (Morales et al. 2022), Cova Foradada and Balma de la Griera (Calafell), Guineu (Font-Rubí) and Abric de la Consagració (Capellades) (Oms et al. 2016; Morales et al. 2019, 2022; Fullola et al. 2020; Vaquero & Picin *pers. comm.*), the Upper Paleolithic sites of Can Manel and Pinyons (Capellades) (Vaquero et al. 2013), the Mesolithic site of Abric Agut (Capellades) (Vaquero et al. 2006), and the Neolithic sites of Can Sadurní and Guixeres del Penedès (Vilobí del Penedès) (Edo et al. 2012; Oms et al. 2021). Despite the diachrony, all these sites supplied chert from this formation, becoming a pole of attraction and a vertebra of the territorial structure over time. Obtaining a multi-technique dataset on SMT chert characterization will fulfil an important need, allowing different researchers to identify this chert type frequently found in the archaeological sites of the NE Iberian Peninsula.

In this work, we develop the first multi-scalar approach to the chert of the Sant Genís Formation (Priabonian,

Cenozoic) of evaporitic origin with a view to obtaining a detailed characterization of the different lithological units yielding it. From a petrographic perspective, Cenozoic cherts of evaporitic origin are characterized by great heterogeneity, the absence of microfossils, and a high presence of post-genetic alterations such as the development of white patina, which frequently make it difficult to undertake a correct archaeological ascription.

SMT chert (Sant Martí de Tous, Barcelona) is found within evaporite lithofacies (sabkha-like), defining a depositional environment comprising shallow saline lakes with low-concentration brines of calcium sulfates, where massive gypsums, gypsiferous marls, carbonate sedimentation, gypsumarenites, and red and gray lutites are deposited, depending on the horizontal location (lake center or margin) and stage (dilution, exposure) (Ortí et al. 2007). SMT chert outcrops are located within lutites, gypsums, marls, and calcarenites. This heterogeneous lithological context motivated our multi-method analysis of their petrographic and geochemical traits, our aim being to explore the homogeneity or heterogeneity among cherts from the same geological formation but different enclosing lithologies. Heterogeneity in evaporitic cherts poses a particular problem when it comes to their macroscopic characterization and ascription to archaeological raw material groups. Determining their diagenetic variability will make it possible to define these groups more precisely and reliably, so that the following analyses (thin section, chemical characterization, etc.) will show the reality of the SMT type chert as a whole rather than sample specificities that can lead to confusion.

We petrographically analyze 46 samples (enclosing rocks and cherts of geological and archaeological origin), of which six chert types representing the main lithologies of the formation are tested by multiple material analyses. Techniques including X-ray diffraction (XRD), magnetic property analysis, portable X-ray fluorescence (p-EDXRF), inductively coupled plasma optical emission spectroscopy (ICP-OES), and neutron activation analysis (NAA) are applied to explore the mineralogical and geochemical variability of the samples. The data obtained are compared with three archaeological chert samples (AR'01-M-Q47-49; AR'02-M-U47-220; and AR'02-M-P53-537) from level M (between  $51.8 \pm 1.4$  and  $55.8 \pm 2.3$  ka BP) of Abric Romaní, which were previously assigned to this formation (Gómez de Soler et al. 2020a), to test the ascription and confirm the validity of this multi-method approach.

The archaeological chert sample AR'01-M-Q47-49 was characterized macroscopically as fine texture, gray translucent color (*N5 Medium Gray*), oxides as inclusions, and laminations as sedimentary structures. Microscopically is formed by micro-cryptocrystalline quartz (50–60%), length-fast chalcedony cementing vugs (1–3%), detrital quartz

(1–3%), secondary gypsum (15%), micrite (10%), clay minerals (5%), and some gypsum pseudomorphs and skeletal grains as relicts of the primary depositional texture. The AR'02-M-U47-220 macroscopically presents a medium texture, brownish opaque color (*5YR 4/1 Brownish Gray*) with oxides. Microscopically is formed of microcrystalline quartz (40–50%), length-fast chalcedony infilling ancient porosities and to a lesser extent replacing the primary depositional matrix (5–20%), secondary gypsum (15–35%), disseminated sparitic carbonates (5–10%), and dissolution and nodulization structures that have not been completely replaced. The AR'02-M-P53-537 was characterized macroscopically as fine texture, gray opaque color (*N5 Medium Gray*), fissures and oxides, and crystal fillings as inclusions. Microscopically is formed by micro-cryptocrystalline quartz (50–60%), length-fast chalcedony cementing vugs (1–3%), detrital quartz (1–3%), secondary gypsum (15%), micrite (10%), clay minerals (5%), and some gypsum pseudomorphs and skeletal grains as relicts of the primary depositional texture. This work aims to fill the gap noted in previous studies on this raw material fundamental to NE Iberia, providing a detailed petrographic and geochemical data catalogue to allow its correct ascription at any archaeological site in the area from the Middle Paleolithic onwards.

## Geological setting

The Sant Genís Formation (Colldeforns et al. 1994) is a Cenozoic unit that forms part of the sedimentary infill of the Ebro Basin, bordered by the Pyrenees and the Basque-Cantabrian Ranges to the north, by the Iberian Range to the south, and by the Catalan Coastal Range to the east. The depression drained mainly by the Ebro River is a Tertiary sedimentary basin with Paleogene deposits formed by erosive processes affecting the bordering ranges (Solé Sabarís 1964).

The Sant Genís Formation is of Priabonian age (upper Eocene) and is part of La Noguera lacustrine system (Anadón et al. 1989), falling within the Upper Gray Lutite unit (Saez 1987). At present, it extends a length of 12 km, with a maximum width of 1.5 km, showing a NE-SW orientation from the locality of Sant Genís (Jorba) through the locality of Fillol (Sant Martí de Tous), and covering a surface area of 5.6 km<sup>2</sup> (Fig. 1). It comprises a succession of 400 m of red sandy lutites, with horizontal lamination and ripples, including occasional limestone layers with charophytes and gastropods (Colldeforns et al. 1994). In geological maps, it is presented as two formations; one formed by red sandstones and marls, and the other by gray sandstones and marls, with local stratified gypsum (IGME 1975).

Silicification outcrops are associated with the unit of red sandy lutites and occasional tabular red sandstones. At the base of the formation, alternating layers of nodular

and laminated gypsums are described, and to the SW of the locality of SMT, this changes to an alternation of massive gypsums with nodular cherts (Ortí et al. 2007).

At its base (NE), the geological section of the region shows the Artés Formation (lower Priabonian), formed by an alternation of marls and red sandstones. Above this lies the Sant Genís Formation, represented at its base by the 20-m-thick SMT gypsum, and towards the top by an 80 m deposit of upper Priabonian marls, red sandstones, and sporadic gypsum. On top (SE of the section), the Intermediate Lacustrine Units (Colldeforns et al. 1994) are located, represented by the Copons Formation (Sannoisian, lower Oligocene), consisting of gray marls, sandstones, and gypsums (Fig. 2).

## Materials and methods

The chert outcrops of the Sant Genís Formation are located to the SW of the town of Sant Martí de Tous. Two sectors with a considerable chert concentration can be differentiated, the sectors of Guinardera and Fillol, which include a total of 14 chert outcrops (eight associated with the former sector and six with the latter). The names of these outcrops relate to the nearest toponyms (see Fig. 1).

A total of 22 geological chert samples were petrographically analyzed in accordance with their enclosing rocks and varying depositional environments. In addition to thin sections, five characterization techniques were applied: X-ray diffraction (XRD), magnetic property analysis, portable energy-dispersive X-ray fluorescence (p-EDXRF), inductively coupled plasma optical emission spectroscopy (ICP-OES), and neutron activation analysis (NAA). These were applied to samples from Perdut 01 (PER-01), Perdut 03 (PER-03), Perdut 04 (PER-04), Mas de Tous (MDT), Cal Calaf 01 (CAL-01), and Fillol 01 (FILL-01).

## Survey and sampling

The cartographic and geological data available for the area were analyzed to identify the different chert-bearing units. Once located, the chert outcrops were registered in a specifically designed database, where their main characteristics (location, accessibility, geological context, etc.) were recorded. In addition, the outcrop locations were imported in a vector format onto a digitized map with geological and cartographic data (scale 1: 50,000) to create a specific cartography of the chert availability in the area.

To provide a quantitative approximation of the layout of the chert, the chert abundance ratio method (CAR method) was applied to estimate the chert input of the Sant Genís Formation to the territory. This methodology has been broadly

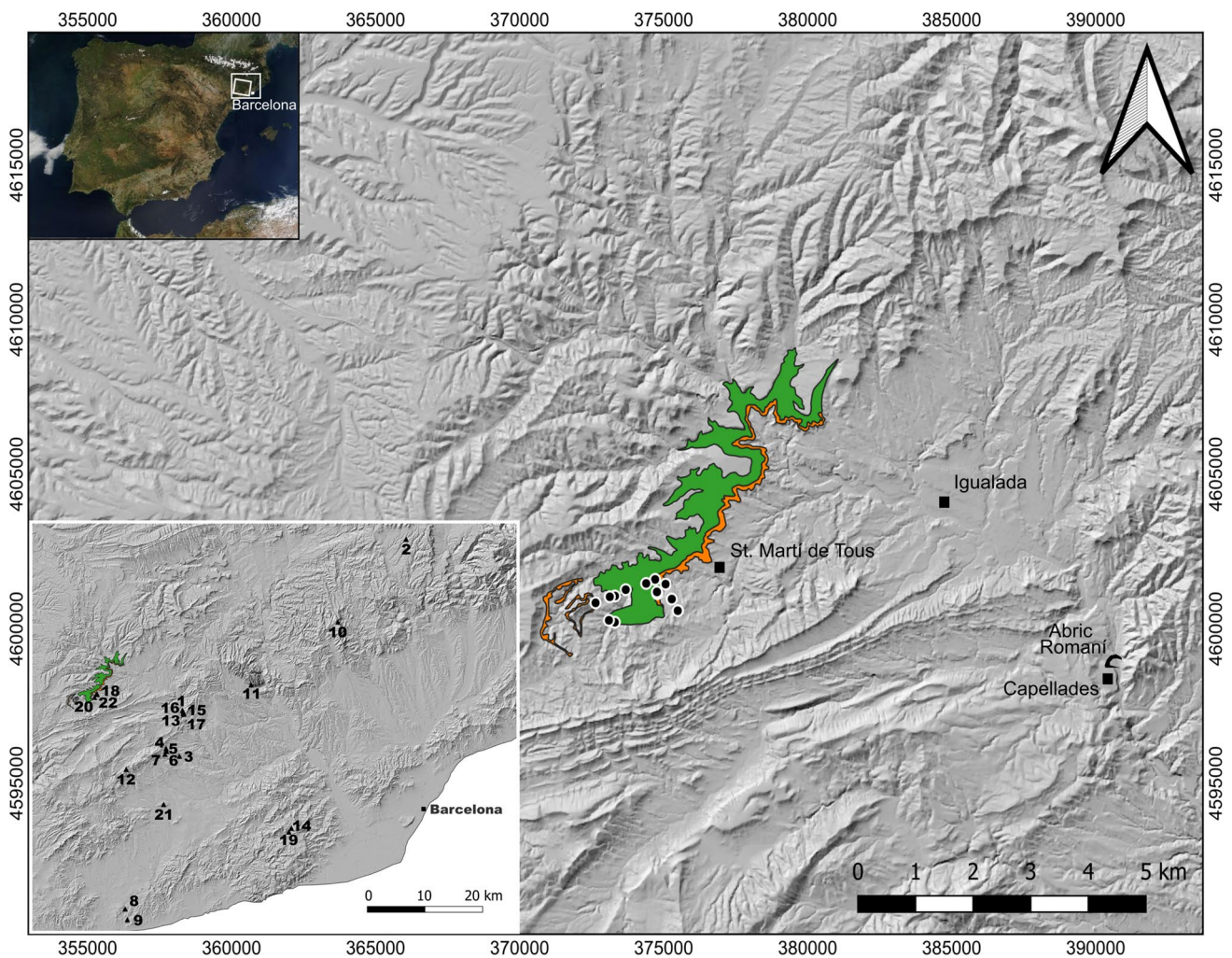


**Fig. 1** Sant Genís Formation (green and orange) in a DEM map with the aforementioned chert outcrops (black dots). To the right is the location of the Abric Romani site. Below left, the main sites mentioned above. 1, Abric Romani; 2, Cova de Teixonerres; 3, La Noguera; 4, La Fàbrica; 5, Mediona; 6, La Canyada; 7, Les Deus; 8,

La Griera; 9, Cova Foradada; 10, Cova Simanya; 11, Cova Gran; 12, Cova de la Guineu; 13, Abric de la Consagració; 14, Esquerda de les Alzines; 15, Can Manel; 16, Abric Agut; 17, Pinyons; 18, Cal Sitjo; 19, Can Sadurní; 20, Vilars de Tous; 21, Guixeres del Penedès; 22, La Guinardera Nord

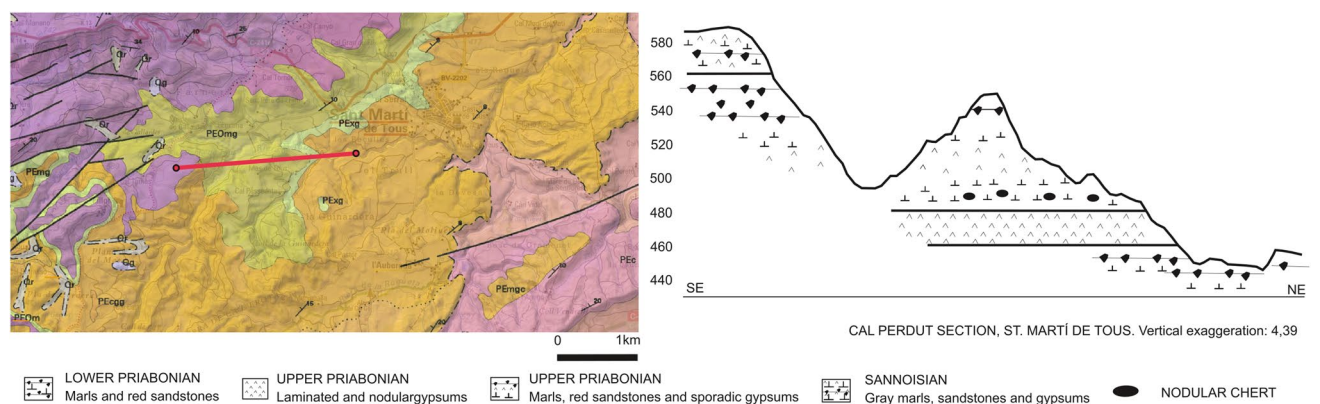


**Fig. 2** Geological section of the Cal Perdut area. Left: location of the section on the 1:50,000 geological map (red line with red dots at each end) (modified from [www.icgc.cat](http://www.icgc.cat)). Right: geological profile according to the topographic base

described by Soto et al. (2018) and successfully applied in previous works (Soto 2015; Gómez de Soler 2016; Gómez de Soler et al. 2019, 2020a, 2020b).

The outcrop sampling resulted in the collection of a total of 40 hand samples housed at the IPHES lithothèque (Lith-IPHES), including all the macroscopic varieties of silicification and enclosing rocks.

## Petrographic analysis

The morphoscopic analysis consisted of naked-eye and stereoscopic microscope (ZEISS Stemi DV4 8-32x) observations. We analyzed external aspects such as the type of support (e.g., block, pebble, preform, core, flake) and the cortical area (presence/absence, type of cortex, morphology, lithological origin), and internal aspects such as the color (using the Munsell Rock Color Book, Munsell Color 2013) and its distribution within the surface, transparency, texture, the presence of sedimentary structures, fissures and fractures, post-depositional alterations, impurities, and the microfossil content (see Soto et al. 2014).

Petrological thin sections were analyzed by polarized light microscopy (Nikon Eclipse E400 POL 40-400x) to determine the mineral composition, textural characteristics, and impurities content, thus analyzing the siliceous matrix as well as noting the presence or absence of relict and authigenic minerals and possible alterations or compactions.

A total of 46 petrographic thin sections were prepared and analyzed at the IPHES-CERCA Geoarchaeology Laboratory; these comprised 22 geological chert samples, 13 enclosing rocks, and 11 archaeological samples.

## X-ray diffraction (XRD)

XRD analyses were performed at the Scientific and Technical Resources Service of the Universitat Rovira i Virgili (URV) in Tarragona (Spain), using a Siemens D5000 diffractometer (Bragg–Brentano parafocusing geometry and vertical  $\theta$ – $\theta$  goniometer) fitted with a curved graphite diffracted-beam monochromator, an incident-beam Soller slit, a  $0.06^\circ$  receiving slit, and a scintillation counter as a detector. The angular  $2\theta$  diffraction range was between  $5^\circ$  and  $70^\circ$ . The data were collected with an angular step of  $0.03^\circ$  at 6 s per step and sample rotation.  $\text{CuK}_\alpha$  radiation was obtained from a copper X-ray tube operated at 40 kV and 30 mA.

Identification of the minerals was achieved by comparison of the XRD diffractogram with the ICDD database (release 2007) using Diffrac<sup>plus</sup> Evaluation software (Bruker-AXS 2009).

Quantitative phase analysis was derived from XRD powder patterns using the Rietveld (Rietveld 1969) software TOPAS (Bruker-AXS 2009). The instrumental contribution was introduced with the fundamental parameter approach (Cheary et al. 2004). The preferred orientation effect was

corrected using the March-Dollase model (March, 1932) (Dollase 1986). For the moganite and calcite phases, the [011] and [104] directions were introduced respectively; for gypsum, the [010] direction was employed. The background for each diffraction pattern was fitted as a 5th-degree Chebyshev polynomial. For every profile, the zero shift and overall scale factor, cell parameters, and Lorentzian contribution to the peak width produced by the crystallite size were refined.

The quantitative phase analysis using the Rietveld method consists in fitting a calculated X-ray diffractogram to the experimental one and minimizing, by the least-square method, the difference between them. All the algorithms that are used in the Rietveld method try to minimize this difference between the intensity at each point of the observed profile ( $I_i$ ) and the calculated intensity at the same point ( $I_{ci}$ ) of the diffractogram. The quantity to be minimized during the refinement is:

$$R_y = \sum_i \omega_i (I_i - I_{ci})^2$$

where  $\omega_i = 1/I_i$ . The sum is performed for all points in the diffractogram. The calculated X-ray diffractogram is obtained from the crystal structure of each phase plus geometrical considerations of the diffractometer.

The following table shows the crystal structures employed for each phase (Table 1).

The weight fraction of a  $w_i$  phase in a system of  $n$  crystalline phases is given by the expression:

$$W_i = \frac{S_i \rho_i V_i^2}{\sum_{j=1}^n S_j \rho_j V_j^2}$$

where  $\rho_i$  is the crystal density,  $V_i$  is the unit cell volume, and  $S_i$  is the refinable scale factor for phase  $i$ . The previous expression is applicable when all phases considered in the sample are crystalline so that:

$$\sum_i W_i = 1$$

## Magnetic properties

A bulk sample (~ 500 mg) from each chert sample was extracted to analyze its magnetic properties. The analyses were carried out using a variable field translation balance (VFTB) and comprised the following sequence: (i) progressive isothermal remanent magnetization (IRM) acquisition curves, (ii) hysteresis loops ( $\pm 1$  T), (iii) backfield coercivity curves, and (iv) thermomagnetic curves up to  $700^\circ\text{C}$  in air. All these analyses were performed at the laboratory of paleomagnetism of the Universidad de Burgos (Spain).

**Table 1** Crystal structures employed for each phase

Composition phase name	System, space group	Crystal parameters	Atomic positions (x, y, z)	Preferred orientation vector	Reference
Quartz	Trigonal P3 <sub>2</sub> 1	a: 4.9120 Å c: 5.4040 Å	Si (0.4700, 0, 2/3) O (0.4150, 0.2680, 0.7860)		(Ogata, Takéuchi, & Kudoh, 1987)
Moganite	Monoclinic I 2/a	a: 8.758 Å b: 4.876 Å c: 10.715 Å β: 90.08°	Si (¼, -0.0092, 0) Si (0.0115, 0.2533, 0.1678) O (-0.0314, 0.0680, 0.2860) O (0.1711, 0.177, 0.105) O (-0.1343, 0.2148, 0.0739)	011	(Miehe & Graetsch, 1992)
Calcite	Trigonal R-3c	a: 4.9900 Å c: 17.0610 Å	Ca (0, 0, 0) C (0, 0, ¼) O (0.2570, 0, ¼)	104	(Sass, Vidale, & Donohue, 1957))
Gypsum	Monoclinic I 2/a	a: 6.5220 Å b: 15.2020 Å c: 5.6790 Å β: 118.4°	Ca (¼, 0.4213, 0) S (¼, 0.9216, 0, 0) O (0.5505, 0.1319, 0.9632) O (0.6671, 0.0223, 0.7582) O (0.4588, 0.1821, 0.3796)	010	(Cole & Lancucki, 1974)

After correcting the hysteresis cycles for their dia/paramagnetic fraction, various rock-magnetic parameters were determined using the *Rock Mag Analyzer* software (Leonhardt 2006). These included  $M_s$  (saturation magnetization),  $M_{rs}$  (remanent saturation magnetization), and  $B_c$  (coercive field). The remanent coercive field ( $B_{cr}$ ) was determined separately from the backfield coercivity curves. In combination with other analyses such as thermomagnetic curves, these parameters are used as indicators of ferromagnetic (*sensu lato*, *s.l.*)—strongly magnetic—mineral concentration and composition in the sample (Evans and Heller 2003). The Curie/Néel temperatures were determined from the thermomagnetic curves following the two-tangent method of Grommé et al. (1969). Another proxy considered was the S-ratio (Bloemendal et al. 1992), which is defined here as  $IRM@0.3\text{ T}/IRM@1\text{ T}$ , taking 1 T as the maximum available applied field. The S-ratio is generally used to constrain the ratio between high-coercivity (e.g., hematite/goethite) and low-coercivity (e.g., magnetite/maghemite) minerals.

### Portable energy-dispersive x-ray fluorescence (p-EDXRF)

Chert samples were analyzed at the Instituto de Ciencia de los Materiales (ICMUV) of the Universitat de València (Spain), using a portable EDXRF spectrometer with an X-ray tube (Moxtek, Inc.) with a silver anode operating in transmission mode at a voltage of 30 kV, a current of 10 A and an acquisition time of 240 s. The spectrometer has a thermoelectrically cooled Si-PIN detector (Amptek, Inc.), with an active area of 6 mm<sup>2</sup>, a 12.5 m beryllium window, and an energy resolution of 165 eV (FWHM @ 5.9 keV). An aluminum collimator collimates the X-ray beam, and the beam diameter on the surface of the sample is about 5 mm.

These elements were fitted together on a mechanical device that enabled us to place the system in front of the analysis point and maintain the same geometry, ensuring the reproducibility of the measurements. The X-ray beam impinged perpendicularly upon the sample, and the tube and detector were placed with an excitation-detection geometry of 45° and a 2 cm sample-detector distance.

The selected samples were left untreated and analyzed at several discrete locations, using relatively flat areas of each chert sample with no cortex or inclusions. Net areas of the K-fluorescence lines generated at each location were calculated by means of the PyMCA analysis software (Solé et al. 2007).

The R environment (R Core Team 2021) and the “ggplot2” package (Wickham 2016) were used to create boxplots of the p-EDXRF counts for major elements in the samples. A principal component analysis (PCA) of the p-EDXRF readings was then performed using the R packages “FactoMineR” (Le et al. 2008) and “factoextra” (Kassambara & Mundt 2017).

### Inductively coupled plasma optical emission spectroscopy (ICP-OES)

This technique involves vaporizing, dissociating, ionizing, and exciting the different chemical components of a sample within an argon plasma. When atoms are de-excited, electromagnetic radiation is emitted within the visible ultraviolet spectrum with characteristic wavelengths for each component. These radiations are separated according to their wavelength, and finally their intensity is measured.

ICP-OES analyses were performed at the Scientific and Technical Resources Service of the Universitat Rovira i Virgili (URV) in Tarragona (Spain), using an inductively coupled plasma optical emission spectrometer (ARCOS FHS16). These analyses consisted of two phases. The first phase was to

dissolve the sample and perform the digestion with an Anton Paar microwave (Space Cube M627). The process was based on a 500 mg ground sample of chert with 2 mL of HNO<sub>3</sub> and 0.5 mL of HF and consisted of 5 min in the microwave. After various steps of five and 10 min with a total of approximately 40 min in the microwave adding 0.5 mL of HF in two stages, we ended with a total of 500 mg of chert, with 2 mL of HNO<sub>3</sub> and 1.5 mL of HF. Afterwards, the sample was fully diluted. The second phase consisted of direct measurement with an ICP spectrometer Spectro ARCOS FHS16. The following parameters were used for element detection: nebulization system cross-flow, plasma power up to 1400 W, pump pitch to 30, refrigerant flow at 13.00 (l/min), auxiliary flow at 1.00 (l/min), nebulization flow at 0.90 (l/min), torch Z at 10.0 (mm), and measurement time of 28.0 (s).

Line plots of the trace element values for each geological chert sample were created in R with “ggplot2,” and ternary plots of Mg, Al, Fe and Al, Ca, Fe with the “ggtern” package (Hamilton & Ferry 2018).

### Neutron activation analysis (NAA)

Using a corundum drill bit, about 80 mg of chert powder was obtained from each sample. The sample powder was then compressed to form pills, adding pure cellulose powder as a binder. The whole set of samples, together with six pills of the Bonn standard, was sent to the research reactor of the Reactor Instituut Delft (Netherlands) and was irradiated there for 10 h with a flux of  $5 \times 10^{12}$  neutrons/(cm<sup>2</sup> s). The emitted radiation from each sample was measured three times during the following 4 weeks applying the routine NAA procedure (Mommsen et al. 1991) at the laboratory of the Helmholtz-Institut für Strahlen- und Kernphysik of the Universität Bonn (Germany). Altogether 30 elemental concentrations were determined. Due to the hardness of the chert samples, a certain number of rubbed-off parts of the corundum drill bit (pure Al oxide) were introduced into the samples, forcing the authors to interpret concentration ratios, instead of absolute concentrations.

Boxplots of the major elements (Na, K, Ca, and Fe) were created in R using “ggplot2.” The measurements of the rare-earth elements in the geological samples were included in a PCA (“FactoMineR” and “factoextra” R packages), and the results from the archaeological samples were included in the PCA space as supplementary individuals.

## Results

### Survey and sampling

The stratigraphic sequence of the Sant Genís Formation allows the vertical succession of the outcrops and the

horizontal relationship among the lithological units through the Guinardera and Fillol sectors to be identified (Fig. 3).

In the Guinardera sector, two sections are described: the Cal Perdut section (including the Cal Perdut 1, 2, 3, and 4 (PER) and Mas de Tous (MDT) chert outcrops) and the Guinardera section (yielding the Guinardera 1, 2, and 3 (GUIN) outcrops).

The Cal Perdut section is an 80 m sequence, presenting at its base 20 m of white marls with decimetric nodular cherts (PER-01), displaying a 20–30% silicification ratio. The overlying layer is formed of 2 m of secondary gypsum, where meganodular cherts are present (PER-02). Metric-sized erratic chert blocks, subangular in shape, confer a 100% chert ratio in this layer. Further up the section is a 15 m layer of calcarenitic rocks with discontinuous tabular chert at the top (PER-03), exhibiting a 10% chert ratio. At the top, a layer made up of alternating marls, green–red lutites, and calcarenitic rocks is found, with chert in both lutite units (the PER-04 and MDT outcrops). Chert appears in decimetric formats with a representation ratio of 10% (Fig. 4).

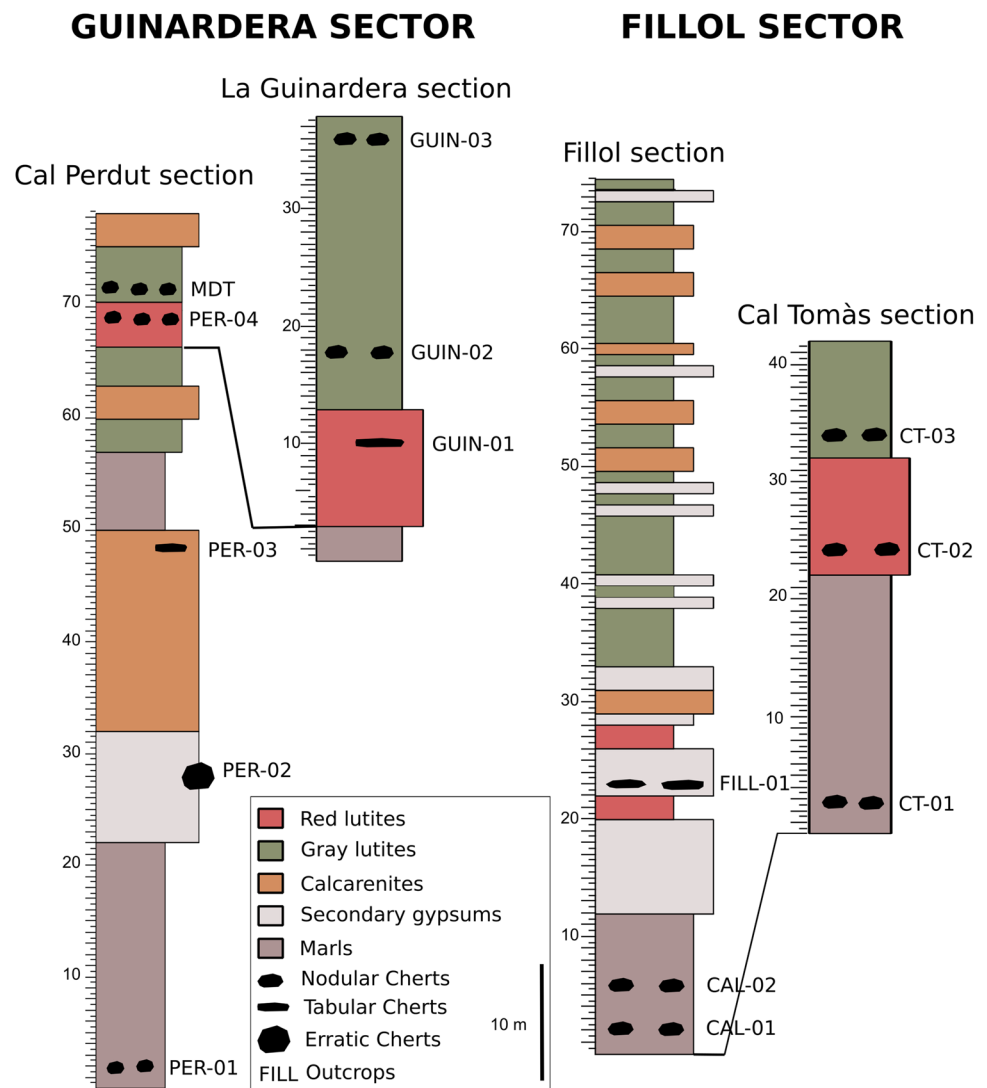
The Guinardera section is a 40 m sequence. At the base, corresponding to the top of Cal Perdut, 10 m of red lutites with sporadic red sandstones are described, yielding discontinuous tabular chert with a 5% silicification ratio (GUIN-01). This unit is followed by 30 m of gray lutites with chert at its base and top (GUIN-02 and GUIN-03), described as decimetric black and gray chert nodules with a 15% silicification ratio in each case (Fig. 5).

In the Fillol sector (Ortí et al. 2007), the Fillol and Cal Tomàs sections are described. The lower unit of the Fillol section is formed of 20 m of gypsiferous marls and secondary gypsum alternating with red and gray lutites and cherts (Cal Calaf (CAL) 01 and 02) with banded stratifications and nodular and meganodular structures. Chert is present in irregular shapes, with decimetric formats and an average chert ratio of 50–60%. Further up, an intermediate unit comprising 10 m of secondary massive gypsums with nodular and meganodular structures yields another chert outcrop (Fillol (FILL) 01). The cherts exhibit elongated nodular shapes and centimetric formats, with a 5–15% representation ratio (Fig. 6). At the top, a 40-m-thick succession of laminated calcarenites alternating with thin units of secondary gypsums without chert is described, covering the whole surface where the village of Fillol is located. This lithological succession, showing a progressive decrease in gypsum with an increase in calcarenites, indicates a shallowing of the sabkha basin, a displacement of its depocenter, and the location of a tidal plane in the Fillol section.

In the Cal Tomàs section, 20 m of white marls with chert nodules (Cal Tomàs 01 (CT-01)) are described at the base, followed by 10 m of red lutites with chert (Cal Tomàs 02 (CT-02)) corresponding to the base of the Fillol section. This is overlain by 10 m of gray lutites with chert nodules



**Fig. 3** Synthetic stratigraphic succession of the Sant Genís Formation in the two identified sectors, showing the vertical and horizontal relation of the different SMT chert outcrops



(Cal Tomàs 03 (CT-03)). CT-01 has a silicification ratio of ca. 10%; CT-02 of 15–25%; and CT-03 of 20–30% (Fig. 7).

Applying the CAR method (Soto et al. 2018) to calculate the siliceous abundance in the territory, a volume of 0.0052 km<sup>3</sup> of chert in an exposed outcrop volume of 0.0207 km<sup>3</sup> was estimated, meaning a chert density in volume of 1.14% for the total exposed volume of the Sant Genís Formation (for more information see Gómez de Soler et al. 2020a).

## Petrographic analysis

### Chert from the replacement of marls

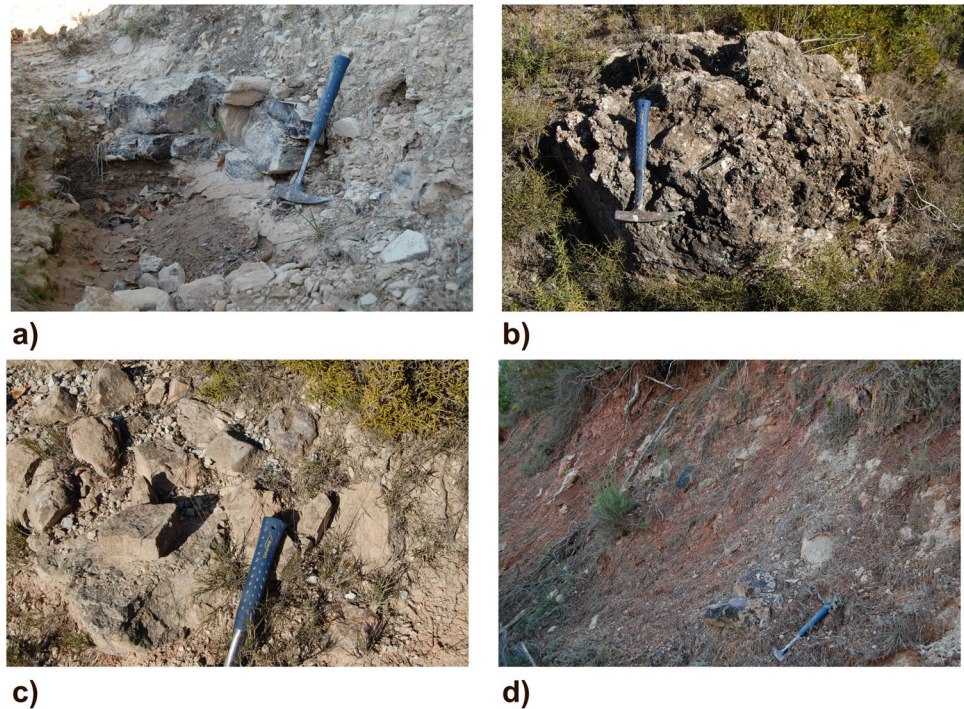
The cherts from PER-01 (Guinardera Sector) and CAL-01, CAL-02, and CT-01 (Fillol Sector) are associated with marly lithofacies. They are macroscopically characterized by fine to very fine textures, with black (*N2 Grayish Black*) and

gray (*N5 Medium Gray*) translucent colors, with some allochemical elements and micritic calcite giving them a mudstone texture, and with some sedimentary structures such as laminations. Microscopically they are formed by microcrystalline quartz (50–60%), length-fast chalcedony cementing vugs (1–3%), detrital quartz (1–3%), secondary gypsum (15%), micrite (10%), clay minerals (5%), and some gypsum pseudomorphs and skeletal grains as relicts of the primary depositional texture (Fig. 8).

### Cherts from the replacement of secondary gypsums

The FILL-01 and PER-02 cherts are a product of the replacement of secondary gypsums. Macroscopically, they are characterized by fine textures, with reddish (*5R 4/2 Grayish Red*; *5R 4/6 Moderate Red*) and black (*N2 Grayish Black*; *N4 Medium Dark Gray*) translucent

**Fig. 4** Chert outcrops of the Cal Perdut section from bottom to top: **a** PER-01. **b** PER-02. **c** PER-03. **d** PER-04



colors, with evaporitic relicts and abundant iron oxides. Microscopically, they are formed by microcrystalline quartz (40%) and spherulitic length-fast chalcedony in matrix, some botryoidal length-fast chalcedony (1–3%), and a mosaic of equant megaquartz cement ancient porosities (1–3%), and secondary gypsum (10%). Iron oxides (15%) and clay minerals (5%) are also described (Fig. 9).

#### Chert from calcarenite facies

Chert from calcarenite facies at PER-03 is macroscopically characterized by fine textures, with bluish-gray (*5B 7/1 Light Bluish Gray*; *N6 Medium Light Gray*) and white (*N9 white*; *N8 Very Light Gray*) colors, and many fissures and gypsum relicts. Microscopically, it is composed of microcrystalline

**Fig. 5** Chert outcrops of La Guinardera section in stratigraphic order from bottom to top. **a** GUIN-01. **b** La Guinardera workshop (LGN). **c** GUIN-02. **d** GUIN-03

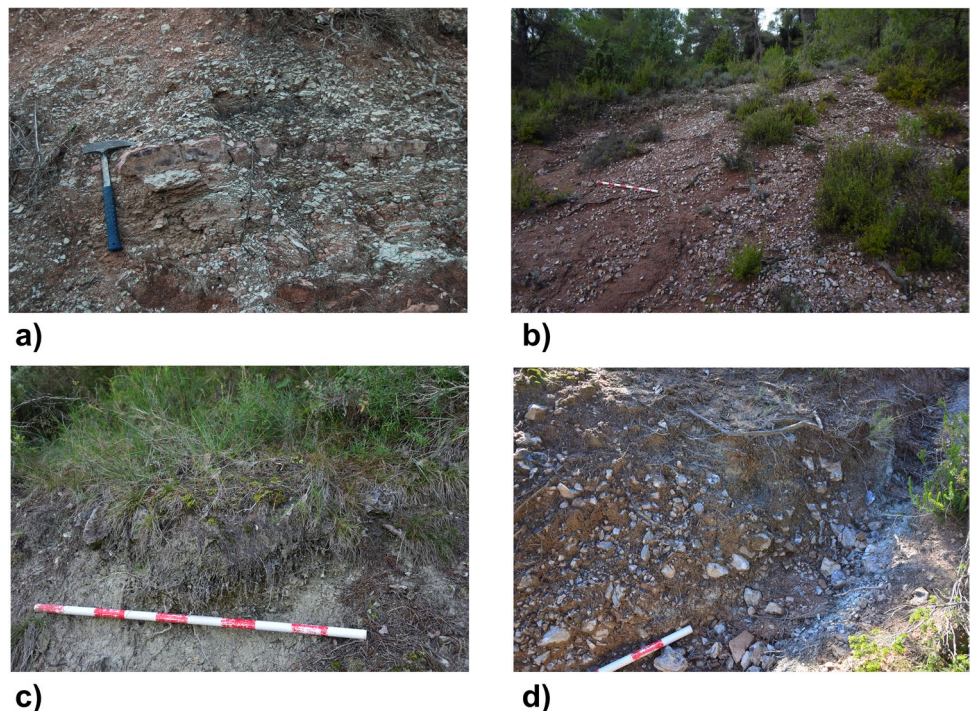
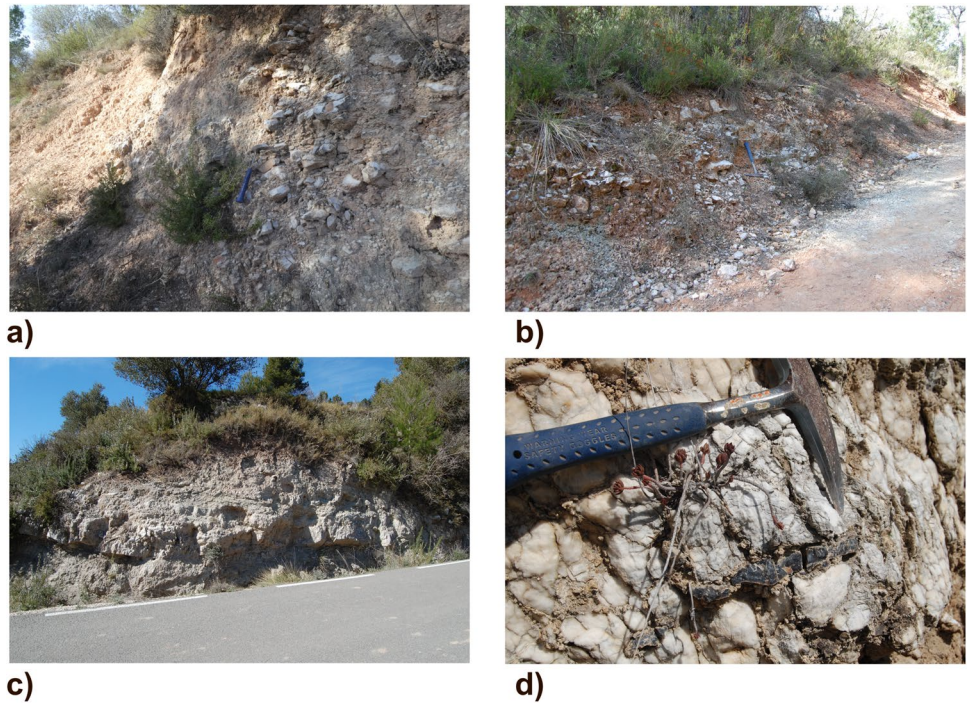


**Fig. 6** Images of the chert outcrops included in the Fillol section from bottom to top: **a** CAL-01. **b** CAL-02. **c** General view of the FILL-01 outcrop. **d** Detail of chert from FILL-01



quartz (40%), spherulitic length-fast chalcedony infilling the dissolution structures of the matrix (15%), and micritic calcite (15%) as a relict of the original matrix, together with secondary anhedral gypsum in veins (20%). A mosaic of

equant megaquartz (5%) as well as ancient cement porosities (vugs and channels), sparitic calcite infilling secondary porosities (10%), disseminated iron oxides (1%), and clay minerals (5%) complete the samples (Fig. 10).

**Fig. 7** Chert outcrops of the Cal Tomàs section in stratigraphic order from bottom to top. **a** CT-01. **b** CT-02. **c** Cal Tomàs workshop. **d** CT-03

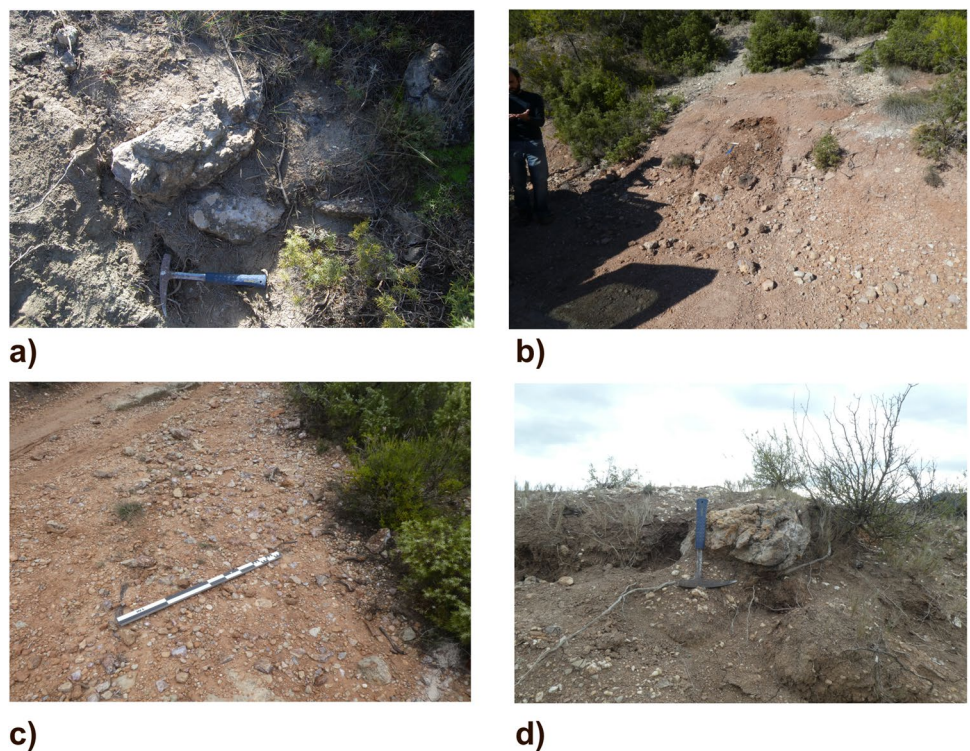
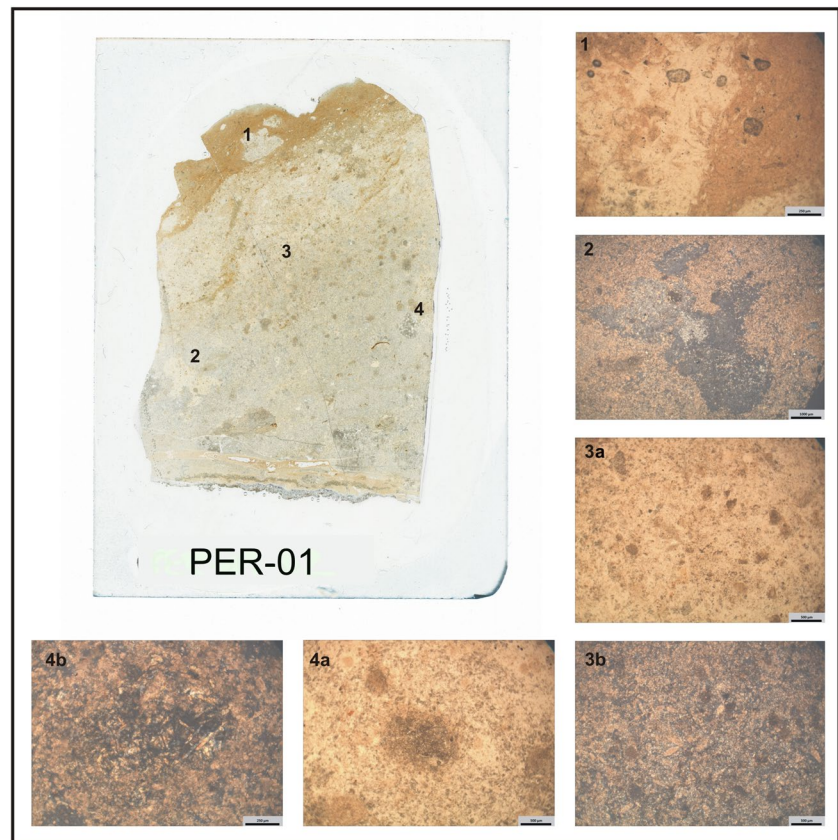


**Fig. 8** PER-01 chert type. (1) With plane-polarized light (PPL), cortex formed by clay and micritic calcite supporting gypsum pseudomorphs cemented by microsparite can be observed. (2 and 3) The internal areas of the silicification, not completely replaced, show a similar depositional texture to the cortex. Images 4a [PPL] and 4b [cross-polarized light, XPL] show aggregates of prismatic anhydrite



### Chert from the replacement of gray and red lutites

Most of the SMT chert outcrops (PER-04, MDT, GUIN-02, GUIN-03, CT-02, and CT-03) are located within gray and red lutites. Macroscopically, these cherts are characterized by fine to medium textures, with blue (*5B 7/1 Light Bluish Gray*; *5 PB 5/2 Greyish Blue* and *5 PB 7/2 Pale Blue*), gray (*N7 Light Gray*) and brownish (*5YR 4/1 Brownish Gray*) translucent colors and evaporite relicts. Microscopically, they are formed of microcrystalline quartz (40–50%), length-fast chalcedony infilling ancient porosities and to a lesser extent replacing the primary depositional matrix (5–20%), secondary gypsum (15–35%), disseminated sparitic carbonates (5–10%), and dissolution and nodulization structures that have not been completely replaced (Fig. 11).

Among the red lutite facies, GUIN-01 displays singular traits. Macroscopically, these cherts present a very fine texture, with a homogeneous red color (*5R3/4 Dusky Red*) and opaque diaphaneity and occasional fissures. Microscopically, they are formed of crypto- and microcrystalline quartz (55%) and abundant clay minerals (up to 40%). As an accessory mineral, iron oxides in the channel porosities (5%) are also present as massive hematite. All these characteristics allow us to define this chert type as a jasper (Fig. 12).

### XRD

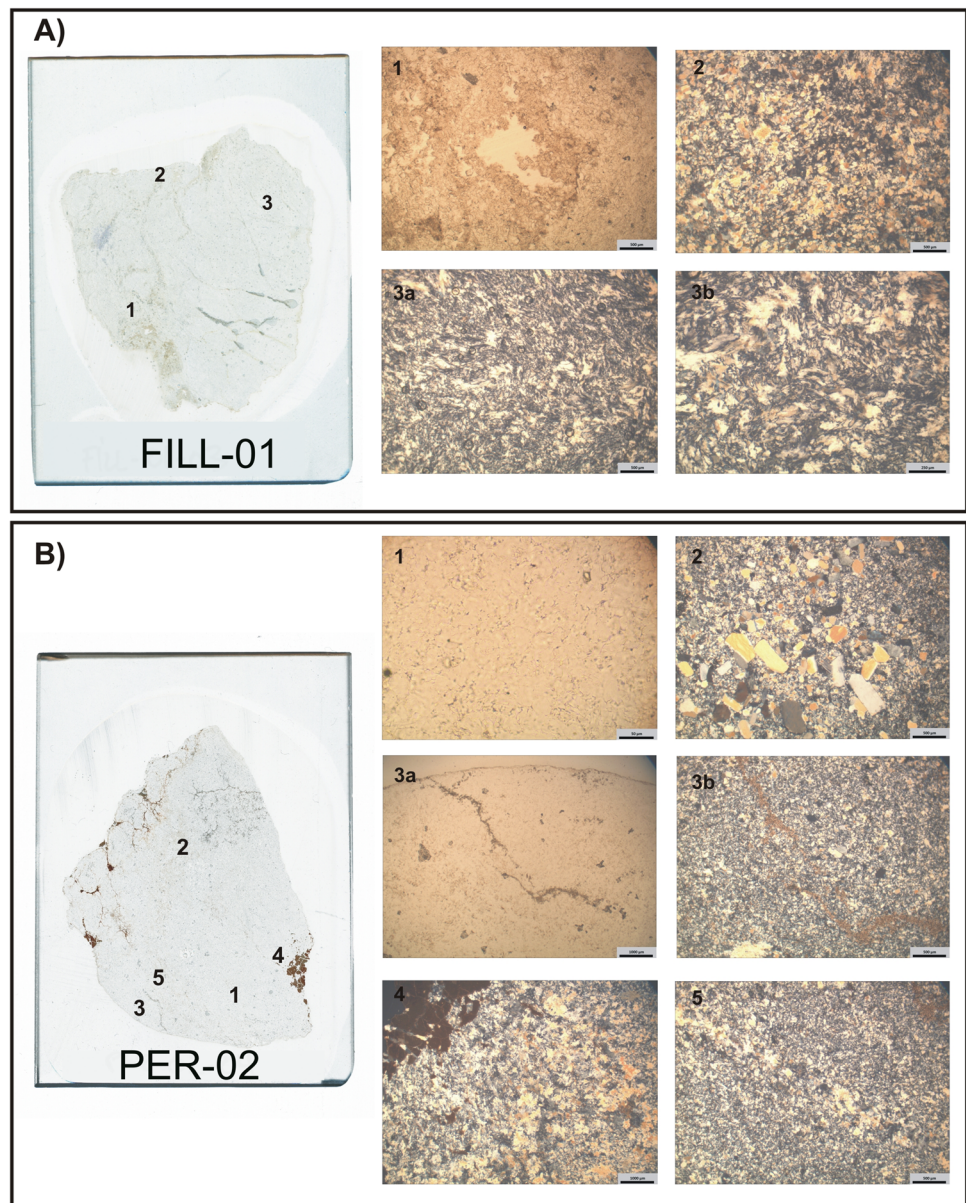
The geological chert samples analyzed by X-ray diffraction show contamination by tungsten carbide (WC), <0.5 wt%, a chemical compound associated with grinding tools to powder samples when these are very hard (e.g., chert) (Fig. SI1). The results of the quantitative phase analysis for each sample are shown in Table 2, together with the conventional Rietveld agreement factor ( $R_{wp}$ ):

The percentages of the quartz phase are very homogeneous (88.6–97.5%). FILL-01 and MDT chert types stand out due to the slight increase in moganite content they show, and PER-03 due to the presence of calcite. These values with quartz and moganite as the only phases are typical of the cherts with fibrous silica (chalcedony) (Graetsch & Grünberg 2012) common among early-diagenetic cherts characteristic of evaporitic formations (Chowns & Elkins 1974). The presence of calcite in PER-03 may be due to a higher subaerial exposure, thus suggesting a more marginal environment, as its enclosing rock indicates.

### Magnetic properties

The application of mineral–magnetic parameters to study the magnetic properties of geoarchaeological materials

**Fig. 9** A FILL-01 chert type. (1) Under PPL, samples show vacuolar porosity (vugs), associated with gypsiferous dissolution structures. Under XPL, the anhedral character of the non-uniform extinction of gypsum crystals (3a and 3b) and subhedral crystals and microcrystalline aggregates is observed; (2) shows typical microstructures of the alabastrine variety. **B** (1) Under XPL, intercrystalline porosity is observed, as well as calcite crystals infilling fissures and bioturbation structures (3a); (3b) detail of calcite crystals and porphyroblastic (2) and vein gypsum (5) microstructures under XPL, in addition to anhedral habits of non-uniform extinction, in a zone where a major accumulation of clay is observed (4)



refers to the identification of iron oxides, hydroxides and some iron sulfides, and minerals generally occurring in trace amounts in many rocks and soils, as well as their variations in concentration and granulometry (Evans & Heller 2003). As expected, the studied cherts are characterized by dominant diamagnetic behavior. Diamagnetism is a property of all matter characterized by very weak magnetization antiparallel to the applied field. When the applied field disappears, diamagnetic materials such as quartz or calcite (typically dominant in cherts) do not retain a remanent or permanent magnetization (Dunlop & Özdemir 1997; Dekkers 2007). Nevertheless, despite being present in very small concentrations, some differences among the studied cherts can be distinguished by virtue of variations in the composition, concentration, and granulometry of their

ferromagnetic mineralogy as we outline below. Table 3 compiles the main magnetic parameters calculated for this sample set.  $M_s$  values vary between  $3.08 \times 10^{-3}$  and  $8.08 \times 10^{-4} \text{ Am}^2\text{kg}^{-1}$  whereas  $M_{rs}$  values range between  $7.59 \times 10^{-4}$  and  $1.11 \times 10^{-4} \text{ Am}^2\text{kg}^{-1}$ .  $B_c$  varies between 134.24 and 9.91 mT, and  $B_{cr}$  between 322.74 and 22.64 mT. Like the  $M_s$  and  $M_{rs}$  values obtained from the hysteresis loops, the variation in the intensity of magnetization can also be inferred from the thermomagnetic curves. The magnetization value of the heating cycle at room temperature ( $J_{30}$ ) ranges between  $1.57 \times 10^{-3}$  and  $3.64 \times 10^{-4} \text{ Am}^2\text{kg}^{-1}$ . In essence, the  $M_s$  and  $J_{30}$  values are rather similar, and under the proviso that the magnetic mineralogy is relatively homogeneous as explained below, they can be considered indicators of the magnetic composition and concentration. As far as domain-state

**Fig. 10** Thin section and microphotography of the PER-03 chert type. (1 and 2) Microcrystalline texture under PPL and XPL. (1a, 1b, and 4) Samples display some vugs and channels cemented by megaquartz and some lenticular gypsum pseudomorphs replaced by fibrous quartz and supported by micritic calcite (3a and 3b)

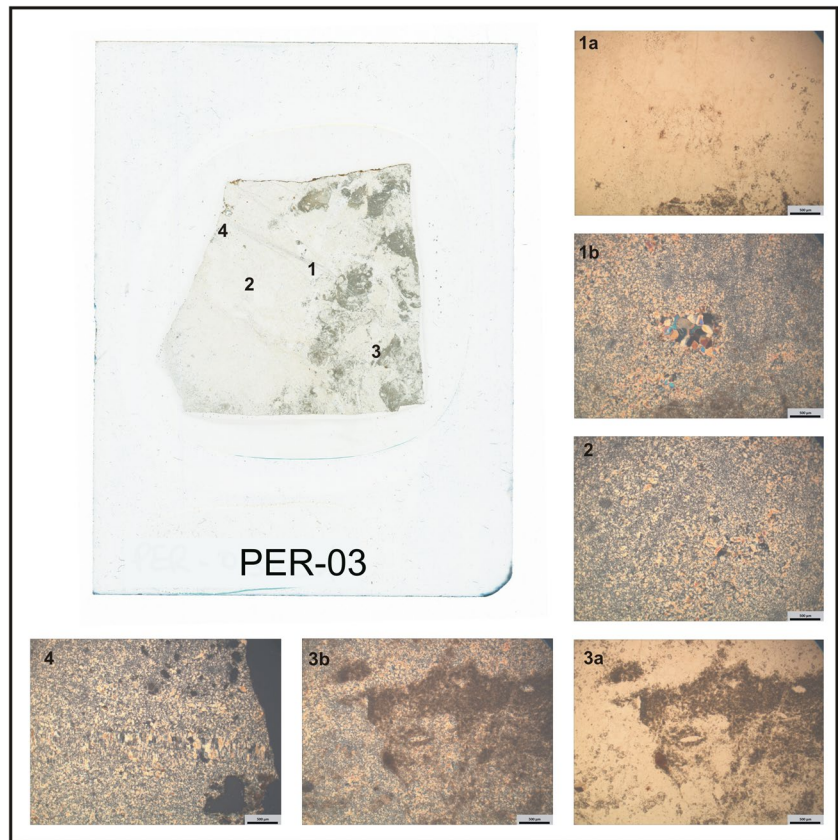


**Fig. 11** Microphotographs of thin sections of the PER-04 chert type. (1 and 2) Under PPL and XPL, its primary depositional texture (secondary gypsum) is replaced by microquartz and fibrous quartz; (3) length-fast chalcedony [accessory wedge of  $1\lambda$ ]; (4) under XPL, disseminated sparitic carbonates, megaquartz cementing the vug porosities, and microquartz in the matrix are observed

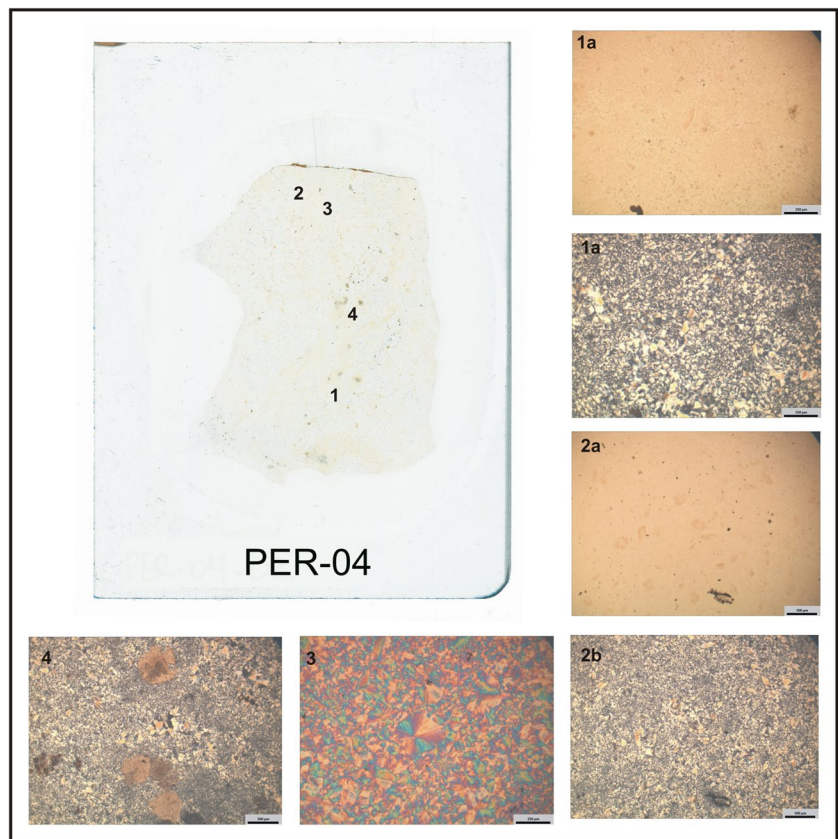
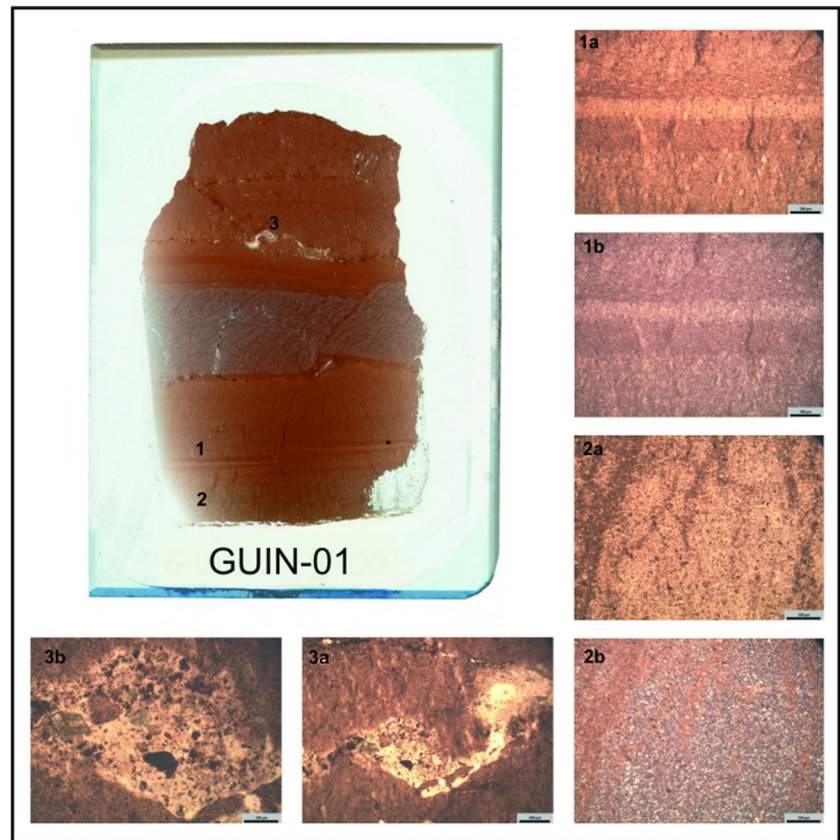


**Fig. 12** GUIN-01 chert type. (1) Laminations resulting from differential clay concentration [PPL and XPL]. (2a) Shrinkage porosity covered by clay and (3a and b) burrow porosity under PPL. (1b and 2b) Under XPL, the replacement of the original lutite matrix by micro- and cryptocrystalline quartz is observed



variations (granulometry) are concerned, we do not consider it realistic to represent the biparametric ratio ( $Mrs/Ms$  vs  $Bcr/Bc$ ) in the so-called Day plot (Day et al. 1977). This is for two reasons: first, its interpretative limitations have been demonstrated (Roberts et al. 1995); second, as detailed below, some cherts also contain variable high-coercivity contributions, and the “Day plot” is theoretically only valid for (titano) magnetite-bearing assemblages.

A diagnostic parameter that qualitatively provides a first approximation to the type of ferromagnetic mineralogy present is the S-ratio (Fig. 13 and Table 3), allowing high- and low-coercivity minerals to be differentiated. The range of variation in this parameter is between 0 and 1 (or  $-1$  depending on the definition considered; see Bloemendal

et al. 1992; Kruiver & Passier 2011). Values near unity indicate a predominance of soft or low-coercivity ferromagnetic minerals (e.g., magnetite), whereas lower values point to a greater contribution from hard or high-coercivity phases (e.g., hematite or goethite). In the present case, the lowest values correspond to FILL-01 (between 0.55 and 0.48) and the PER-04 sets (between 0.43 and 0.65). The other four chert types display values from 0.85 to 1.00, indicating the predominant contribution of a low-coercivity mineral to magnetization. Although S-ratio values close to 1 are often interpreted as representing only low-coercivity minerals, this does not necessarily mean that hematite is totally absent (Bloemendal et al. 1992). Therefore, the interpretation of the S-ratio is not definitive, and the support of additional rock-magnetic analyses is required, as provided here. In any case, the S-ratio is a valid proxy as a first approximation for differentiating between soft and hard ferromagnetic minerals.

Although the magnetization is mostly dominated by a soft mineral, the occurrence of a high-coercivity phase identified in certain types of chert in the S-ratio is also confirmed by other experiments. The IRM acquisition curves of the FILL-01 (Fig. 14a) and PER-04 groups (Fig. 14d) do not reach saturation up to 1 T. That is, the magnetization continues to increase despite the increase in the applied field. The hysteresis loops of these types of chert are clearly wasp-waisted, indicative of the coexistence of low and high-coercivity

**Table 2** Quantitative phase analysis by X-ray diffraction and the conventional Rietveld agreement factor

Sample	Quartz (%)	Moganite (%)	Calcite (%)	$R_{wp}$
CAL-01	97.1	2.9	-	17.09
FILL-01	88.6	11.4	-	19.18
PER-01	95.4	4.6	-	17.5
PER-03	97.5	-	2.5	17.8
PER-04	93.8	6.2	-	17.7
MDT	90.5	9.5	-	18.65

**Table 3** Magnetic properties of the six types of chert analyzed. From left to right: sample code, *Ms* (saturation magnetization), *Mrs* (remanent saturation magnetization), *Bc* (coercive field), and *Bcr* (remanent coercive field) and their respective ratios. *S-ratio* (ranging from 0 to 1), *J<sub>30</sub>* (magnetization value at room temperature or 30 °C taken from the heating cycle of the thermomagnetic curves), *T<sub>c</sub>* (Curie temperature). *Ms* and *Mrs* are expressed in Am<sup>2</sup>kg<sup>-1</sup>. *Bc* and *Bcr* are measured in millitesla or mT. “*N. Int.*” not interpretable

Sample code	<i>Ms</i>	<i>Mrs</i>	<i>Bc</i>	<i>Bcr</i>	<i>Mrs/Ms</i>	<i>Bcr/Bc</i>	<i>S-ratio</i>	<i>J<sub>30</sub></i>	<i>T<sub>c</sub></i> (°C)
CAL-01_a	1.32E-03	3.72E-04	16.06	27.25	0.28	1.70	0.93	1.05E-03	550
CAL-01_b	<i>N. Int.</i>	<i>N. Int.</i>	<i>N. Int.</i>	<i>N. Int.</i>	<i>N. Int.</i>	<i>N. Int.</i>	<i>N. Int.</i>	<i>N. Int.</i>	<i>N. Int.</i>
FILL-01_a	1.06E-03	3.31E-04	30.24	64.04	0.31	2.12	0.55	7.70E-04	560, 675
FILL-01_b	1.44E-03	3.52E-04	28.25	309.02	0.24	10.94	0.48	7.51E-04	580, 675
MDT_a	1.86E-03	3.58E-04	11.94	28.09	0.19	2.35	1.00	1.13E-03	560
MDT_b	<i>N. Int.</i>	<i>N. Int.</i>	<i>N. Int.</i>	<i>N. Int.</i>	<i>N. Int.</i>	<i>N. Int.</i>	<i>N. Int.</i>	<i>N. Int.</i>	<i>N. Int.</i>
PER-01_a	1.38E-03	3.90E-04	15.88	27.29	0.28	1.72	1.00	1.08E-03	550
PER-01_b	<i>N. Int.</i>	<i>N. Int.</i>	<i>N. Int.</i>	<i>N. Int.</i>	<i>N. Int.</i>	<i>N. Int.</i>	<i>N. Int.</i>	<i>N. Int.</i>	<i>N. Int.</i>
PER-03_a	1.44E-03	2.95E-04	18.22	28.04	0.20	1.54	0.95	7.41E-04	580
PER-03_b	<i>N. Int.</i>	<i>N. Int.</i>	<i>N. Int.</i>	<i>N. Int.</i>	<i>N. Int.</i>	<i>N. Int.</i>	<i>N. Int.</i>	<i>N. Int.</i>	<i>N. Int.</i>
PER-03_c	8.08E-04	1.11E-04	9.91	29.05	0.14	2.93	0.98	3.64E-04	<i>N. Int.</i>
PER-03_d	1.56E-03	1.37E-04	12.18	22.64	0.09	1.86	0.85	6.44E-04	580, 675
PER-04_a	1.23E-03	4.25E-04	33.59	58.53	0.35	1.74	0.65	8.16E-04	580, 675
PER-04_b	3.08E-03	5.26E-04	17.02	201.53	0.17	11.84	0.56	1.57E-03	580, 675
PER-04_c	1.36E-03	7.59E-04	134.24	322.74	0.56	2.40	0.43	1.22E-03	675

minerals (Roberts et al. 1995; e.g., Fig. 14b and e). As expected, the highest *Bc* and *Bcr* values coincide with the groups (FILL-01 and PER-04) where the presence of high-coercivity minerals is most evident (Table 3). Among the generally weak magnetism of the studied collection, the other cherts are dominated by low-coercivity minerals (e.g., Fig. 14g–i).

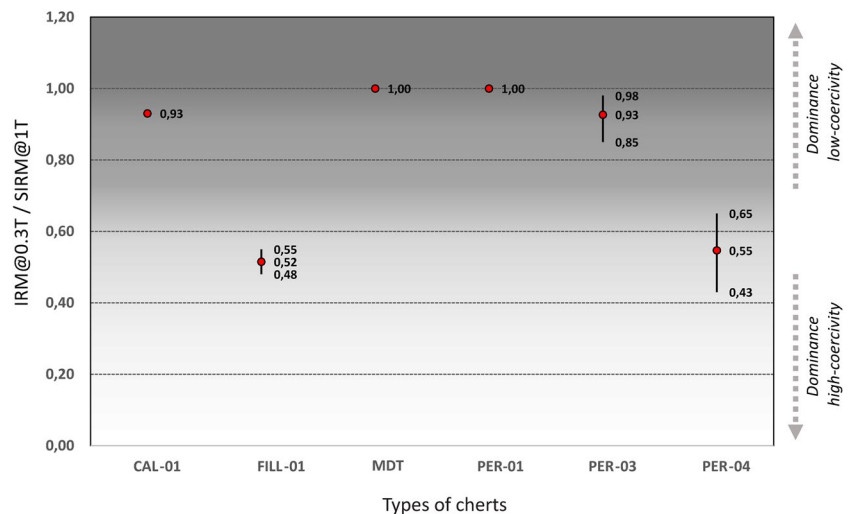
These results are consistent with those observed in the thermomagnetic curves. With a view to obtaining smoother diagrams more amenable to interpretation, a three to five-point running mean was applied to the thermomagnetic curves. The thermomagnetic curves for most samples exhibit a drop in the heating cycle between 550 and 580 °C, consistent with the Curie temperature (*T<sub>c</sub>*) of magnetite or of magnetite with a small amount of isomorphous substitution (Fig. 14i). Exceptionally, the FILL-01 samples exhibit an increase in their heating cycles from

400 to 420 °C, indicating the creation of magnetite during the laboratory heating (e.g., Fig. 14c). During the cooling a major increase in magnetization is found in these samples between 580 and 500 °C, indicating that additional secondary magnetite is created during the experiment. The high-coercivity phase observed in the IRM curves, hysteresis loops, and the *S-ratio* of the FILL-01 and PER-04 samples is hematite, according to the *T<sub>N</sub>* of around 660–675 °C detected in their thermomagnetic curves (Fig. 14c and f).

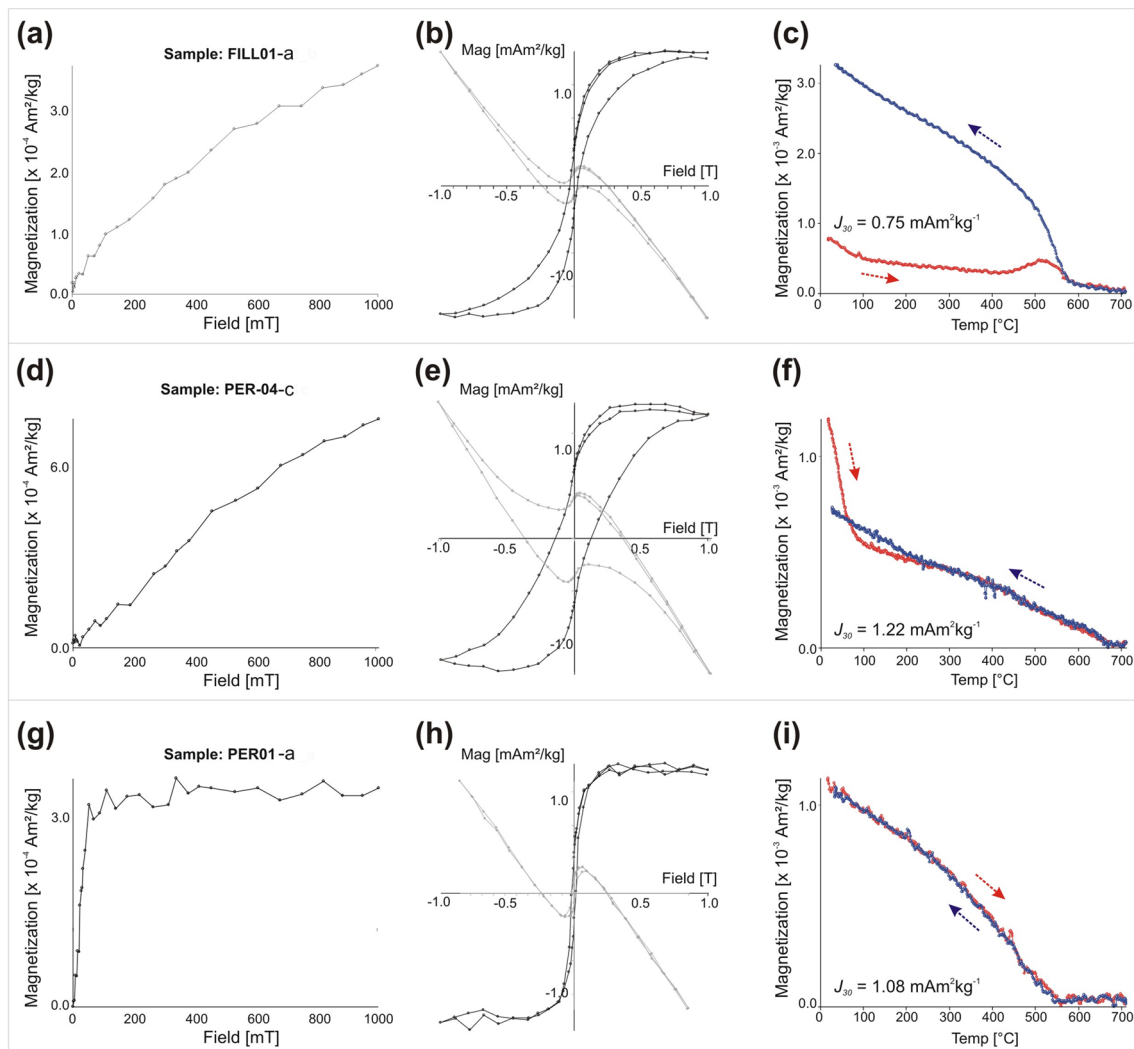
**p-EDXRF**

Table 4 shows the areas of the K-fluorescence lines of the elements detected in the spectra. The presence of W and Ni in the XRF spectra is not taken into account since both elements are present due to the milling process.

**Fig. 13** *S-ratio* values (Bloemendal et al. 1992) for the types of chert studied. Unity (the maximum value) represents a predominance of low-coercivity ferromagnetic minerals. Lower values represent the predominance of high-coercivity ferromagnetic minerals. In those cherts with at least two values per type of chert, the mean value is also shown







**Fig. 14** Representative examples of three chert types studied. Left panels (a, d, g) are progressive IRM acquisition curves. Central panels (b, e, h) are hysteresis cycles, both uncorrected (gray) and corrected (black) for their dia/paramagnetic fraction. Right panels (c, f, i)

are thermomagnetic curves up to 700 °C. Heating (cooling) cycles are denoted by red (blue) colors and their respective arrows. The intensity of magnetization is indicated for each panel

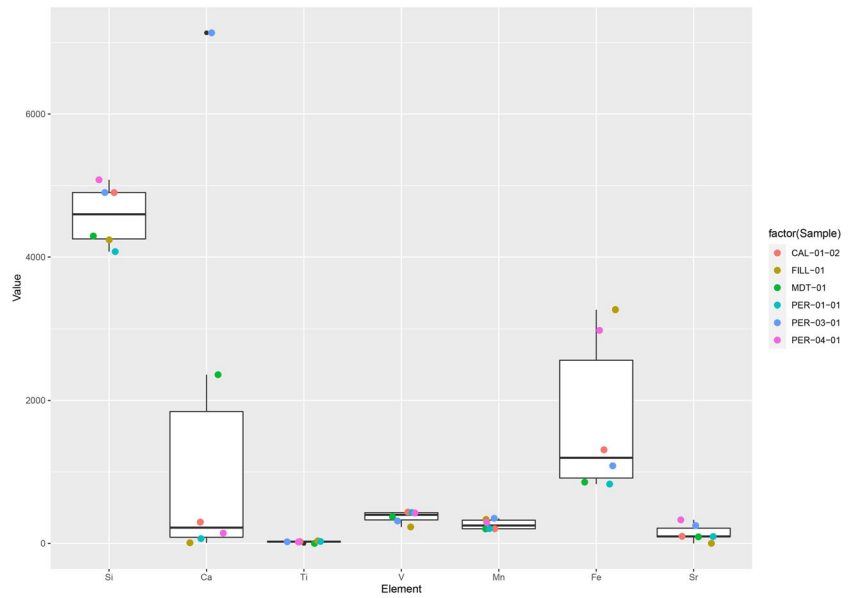
Statistically, according to the intensity of the chemical elements analyzed, the boxplot shows that the six geological samples have homogeneous values. Exceptions are the value of Ca for PER-03, coherent with its enclosing rock consisting of calcarenites (as X-ray diffraction revealed), and the

higher presence of Fe in samples FILL-01 and PER-04, as already shown by magnetic property analysis (Fig. 15). Also, the silica content shows that cherts from non-marginal positions within the sabkha (gypsiferous marls and gypsums) have a lower Si content, probably associated with

**Table 4** K-fluorescence lines of the elements detected in the spectra by means of p-EDXRF

Sample	Si	Ca	Ti	V	Mn	Fe	Sr
CAL-01	4901.1	297.9	25.2	438.6	204.5	1309.1	99.3
MDT	4293.6	2359.2	0.4	374.0	202.7	857.1	92.2
FILL-01	4239.7	9.4	35.6	230.2	335.7	3266.7	1.0
PER-01	4075.5	66.8	27.5	431.7	206.7	829.7	95.9
PER-03	4903.1	7134.9	23.2	313.5	350.7	1085.4	251.3
PER-04	5079.8	143.8	20.4	426.5	294.2	2978.5	329.3

**Fig. 15** Boxplot with all samples by element and value given by p-EDXRF



the process of silica precipitation and replacement (Ortí et al. 2007).

The PCA (components 1–2), representing 68.1% of the variance (Fig. 16a), highlights the major iron content in PER-03 and FILL-01. Also notable is that PER-03 and PER-04 are grouped according to their calcarenitic and lutitic enclosings. Likewise, MDT and CAL-01 are grouped due to their content in V. Lastly, PER-01 is revealed to be the most homogeneous in chemical composition. According to the PCA (56.8% of the variance) (Fig. 16b), the positive axes of components 1 and 3 are consistent with the previous PCA (components 1 and 2) (Fig. 16a). The negative axes again group the CAL-01, PER-01, and MDT samples according to their V content and the homogeneity in their chemical composition.

**ICP-OES**

A total of 24 trace elements were identified by means of ICP-OES. However, the Cr and Cd values were below the detection limits, and Ba was present only in samples CAL-01 and MDT. The P, V, Ag, Pb, Ga, and In values were obtained as a range (Table 5).

The values of Fe and Ca also show the similarities and differences among chert types revealed by this analytical technique. The Ca content is high for PER-03, as is the Fe content for the FILL-01 and PER-04 samples (Fig. 17). The Ca values for PER-04 and CAL-01 are probably due to the context of their formation (lake margin), which may have undergone several subaerial exposure episodes or post-depositional alterations. The higher values for Na in PER-01

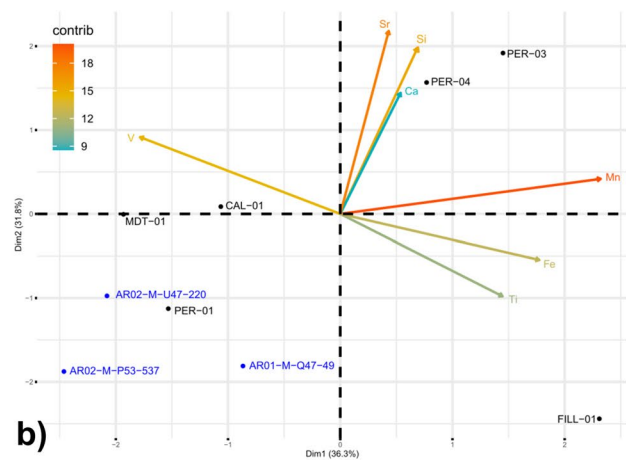
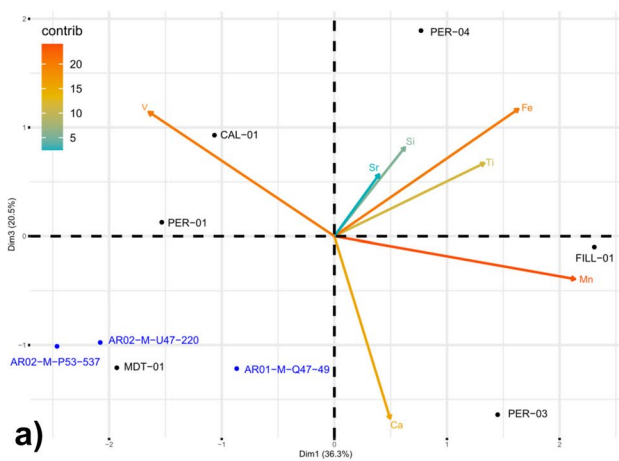


**Fig. 16** **a** PCA of the geological samples with 68.1% of the variance (components 1 and 2); **b** PCA of the geological samples with 56.8% of the variance (components 1 and 3).

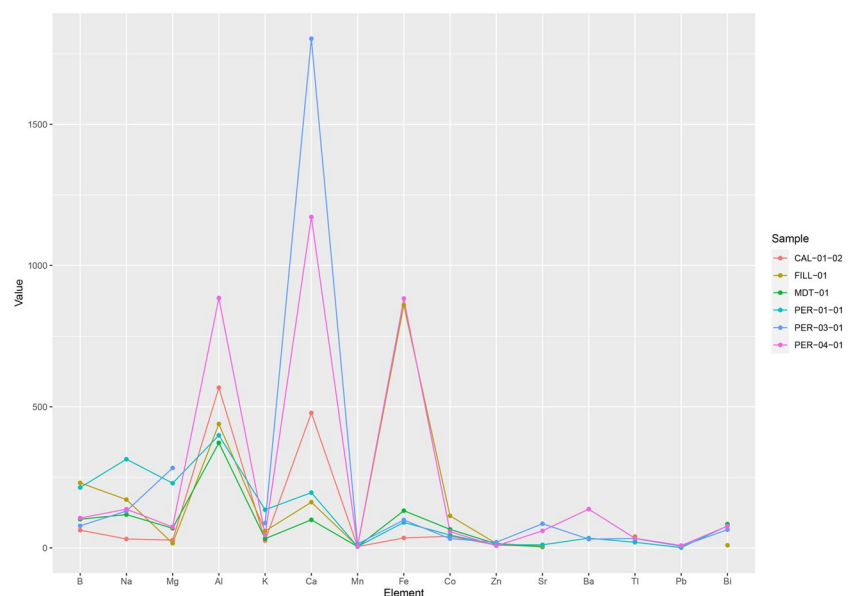
**Table 5** Trace elements in ppm detected by ICP-OES in the geological chert samples

Element	CAL-01	FILL	PER-01	PER-03	PER-04	MDT
Trace elements (ppm)						
Fe	35.18	859.85	90.19	98.94	882.74	131.81
Cu	<0.001	<0.001	<0.001	<0.001	<0.001	<0.001
Mg	27.51	16.52	229.30	283.20	74.23	69.63
Na	31.65	171.24	314.27	130.69	137.19	117.97
K	25.89	59.50	135.09	88.40	45.84	32.70
Ca	478.26	162.02	195.89	1803.47	1171.71	99.48
Zn	9.85	15.67	11.11	20.06	7.36	14.44
Ni	473.97	2169.76	528.01	279.97	542.26	710.98
Mn	4.53	5.42	4.71	13.85	5.71	4.51
Cr	<DL	<DL	<DL	<DL	<DL	<DL
P	<0.002	<0.002	<0.002	<0.002	<0.002	<0.002
V	<0.001	<0.001	<0.001	<0.002	26.88	<0.001
Ag	<0.001	<0.001	<0.001	<0.001	<0.001	<0.001
Al	567.78	439.232	398.88	> 24	884.60	372.42
Co	41.10	113.67	45.53	32.83	57.50	65.69
Pb	<0.006	<0.006	1.10	5.80	8.41	<0.006
Ba	<DL	<DL	34.39	31.18	137.42	<DL
Bi	84.70	9.21	77.71	64.58	76.88	84.02
B	62.79	230.45	213.93	78.27	105.75	101.58
Cd	<DL	<DL	<DL	<DL	<DL	<DL
Ga	<0.001	<0.001	<0.001	<0.001	<0.001	<0.001
In	<0.002	<0.002	<0.002	<0.002	<0.002	<0.002
Sr	5.60	5.97	10.95	85.59	60.38	3.51
Tl	21.56	40.12	19.93	33.21	33.88	23.28

and FILL-01 are coherent with the enclosing lithofacies, gypsiferous marls, and secondary gypsums, respectively.

The ternary Mg–Al–Fe graph (Fig. 18a) shows the PER-01 sample (within gypsiferous marls) as separated from the rest, which could indicate a greater burial depth. The rest of

the enclosing rocks are either shallower (gypsum) or marginal (calcarenites and lutites). The ternary plot for Al–Ca–Fe content groups cherts according to their Fe content (FILL-01 and PER-04) and is consistent with the results observed from the magnetic properties (Fig. 18b).

**Fig. 17** ICP-OES line plot of the trace element values for each geological chert sample

**NAA**

A total of 30 element concentrations were measured by NAA, including trace, major, and rare-earth elements (Table S11). Determining the content of diagenetically immobile rare-earth elements (REE) in chert provides information about the formation environment of the chert deposits (Murray et al. 1990; Murray 1994 and references therein). Important are especially the shale-normalized concentrations of  $Ce_n$ ,  $La_n$ , and  $Nd_n$ , all measurable with NAA. The so-called Ce-anomaly measures the shale-normalized concentrations of Ce against La and Nd [ $Ce_n/Ce_n^* = 3 Ce_n / (2 La_n + Nd_n)$ ], sometimes also logarithmically (Piper & Bau 2013). Also in use is the correlative ratio  $La_n/Ce_n$ . Values of  $Ce_n/Ce_n^* < \sim 0.8$  and  $La_n/Ce_n > \sim 1$  point to Ce depletion and indicate pelagic, open-ocean depositional environments, whereas values of  $Ce_n/Ce_n^* > \sim 0.8$  and  $La_n/Ce_n < \sim 1$  are found for continental margin environments (Malyk-Selivanova et al. 1998). If an archaeological artifact differs in these ratios from a geological deposit, it certainly has a different origin.

In Fig. 19, the Ce-anomaly is shown as a function of the ratio  $La_n/Ce_n$ . As shale normalization, the concentration values of the world shale average (WSA) as given in Piper & Bau 2013 are taken. The large  $1\sigma$  uncertainties reflect the large measurement uncertainties (errors). As specified above, the high Ce-anomaly values as well as the low  $La_n/Ce_n$  ratios indicate a continental margin environment for the formation of the geological chert samples.

Plotting the major elements obtained by NAA highlights the following (Fig. 20): (1) a higher Na content is found in PER-01 compared with the rest of the cherts, emphasizing the absence of Na in the FILL-01 chert type, despite this having secondary gypsum as a bedding rock;

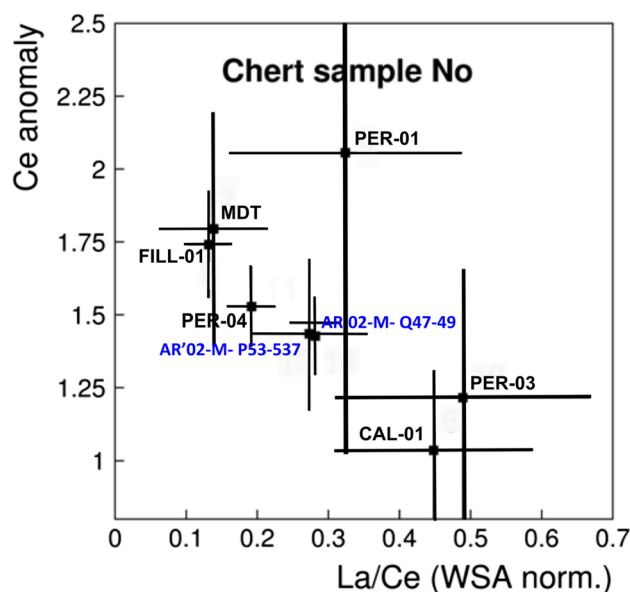


Fig. 19 NAA data:  $Ce\text{-anomaly} = f(La_n/Ce_n)$

(2) the PER-01, PER-03, and MDT cherts show a high K content; (3) the high Ca content of PER-03 is justified by its lower silicification, reflecting the presence of Ca from its host (calcarenites) and consistent with the presence of Ca phases according to X-ray diffraction, as also observed in the ICP-OES and p-EDXRF analyses; (4) as regards Fe content, differences are observed in PER-04 and FILL-01 with respect to the rest of the samples, as consistent with magnetic property analysis, ICP-OES and p-EDXRF.

NAA-REE plotting shows a great dispersion of values, the values being higher in PER-04 than in the rest of the samples (Fig. 21). The PCA (components 1–2; 92.6% of

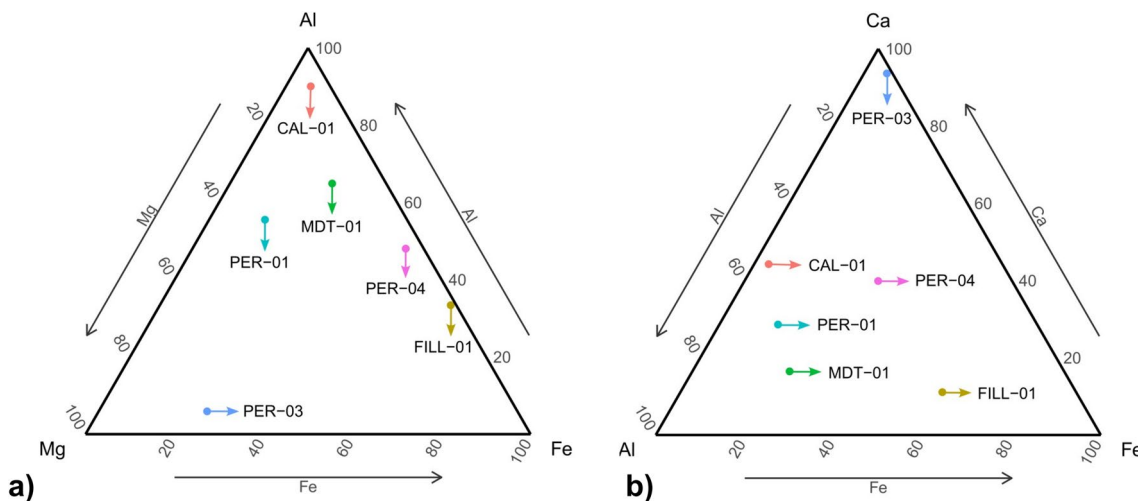
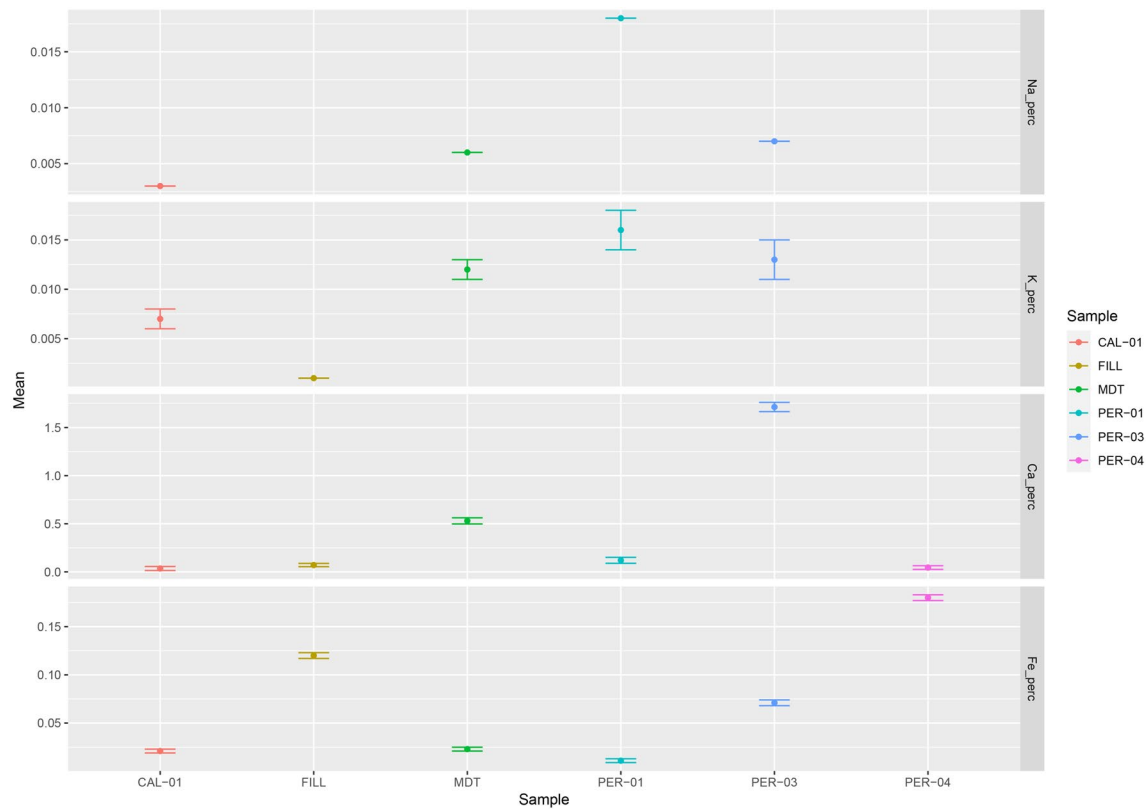


Fig. 18 Ternary plots according to **a** Mg–Al–Fe content; **b** Al–Ca–Fe content



**Fig. 20** Plot of the major elements of the NAA

the total variance) of the REE differentiates the PER-04 and FILL cherts from the rest of the samples according to their higher REE content (Fig. 22). Nevertheless, it seems that what we are observing represents different stages in the silicification process. At this point, it suggests that the composition of the bedrock does not play much of a role. Considering the geological map of the area (IGME 1975), the presence of REE corresponds to the Triassic and Paleozoic materials in the region. The Cenozoic materials seem to be riding on a reverse fault and to have been placed on top of the Paleozoic and Mesozoic materials, the former probably being of granitic origin.

## Discussion

From a macroscopic point of view, it is difficult to associate the different SMT chert varieties with each of the lithofacies in the Sant Genís Formation. First of all, it is important to perform an exhaustive and systematic field work surveys. Secondly, the elaboration of columns and

stratigraphic profiles, and the calculation of the chert ratio for each outcrop and formation. In this first stage, we were able partially to identify, quantify, and delimit the macroscopic variability of this key SMT chert type. In addition, the petrographic analysis of the geological samples allowed us microscopically to differentiate chert varieties of the SMT chert type by their quartz features, mineral components, and preserved sedimentary structures in accordance with the embedding lithology. With this background, we have been able to propose a multi-technique study to assess whether these varieties of the SMT chert type were indeed distinguishable through a variety of techniques of characterization and materials science. Considering the challenge posed by the problems associated with equating the macroscopic scale with the microscopic scale, the idea is to test whether the use of these techniques will lead to a greater and easier characterization of archaeological assemblages. On the other hand, the comparison of these techniques will allow us to evaluate their viability and which ones can be the most useful for archaeological purposes.

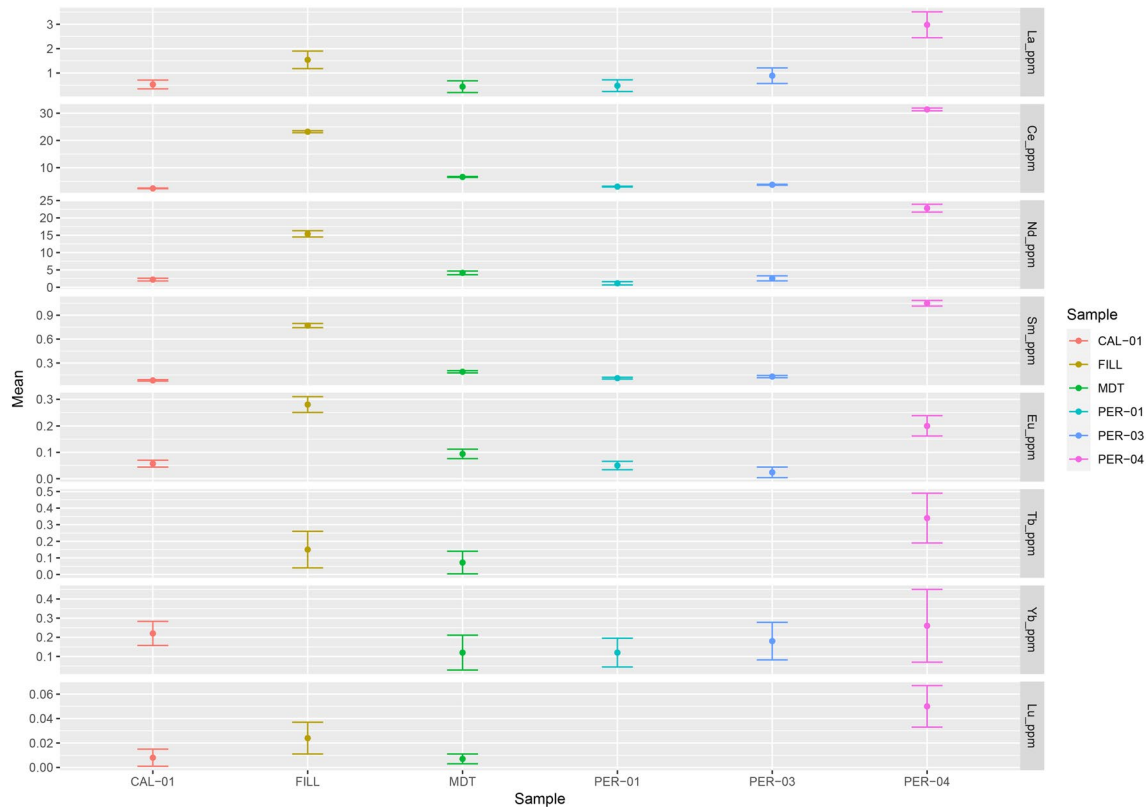


**Fig. 21** Plot of the REE elements from the NAA

### Multi-technique comparison

The nature of the enclosing deposits in the saline lakes of the Sant Genís Formation makes it difficult to differentiate among silicified materials. Our multi-technique approach provides with the insights to relate the geochemical composition with the enclosing lithofacies, their stratigraphic positions, and associated paleoenvironments within the geological formation.

Nevertheless, this work has identified similarities and differences among some of the chert varieties of the SMT chert type relating to the concentration of Fe and Ca. The XRD results clearly differentiate those chert varieties rich in calcite (PER-03) from others. These results are consistent with the p-EDXRF and with the nature of the enclosing rocks. The presence of a higher Ca concentration has to do with the preservation of the original embedding trait, calcarenites from the marginal environments of the evaporite basin, as pointed out by several authors for chert formations (Knauth 1994; Ortí et al. 2007, 2014).

The analysis of the magnetic properties has provided interesting data but being a relatively unfamiliar technique in sourcing lithics, a brief background information and its relevance is added to help the reader. Mineral–magnetic analyses mainly focus on the characterization of the composition

(a specific type of mineral), concentration, and granulometry of ferromagnetic mineralogy. There are several types of ferromagnetism: ferro-, ferri-, and antiferromagnetism (Evans & Heller 2003). For the scope of this study, we will refer here to ferromagnetism (*sensu lato*, *s.l.*) in reference to materials with very large magnetic moments in applied fields (Dekkers 2007). Ferromagnetism is a property of a few minerals such as iron oxides (e.g., magnetite or hematite), iron hydroxides (e.g., goethite), and iron sulfides (e.g., greigite or pyrrhotite) capable of retaining a memory or remanence of the direction and/or intensity of a magnetic field even when this is no longer present. That is the basis of paleomagnetism. In other substances (diamagnetic and paramagnetic), a very low-magnetic moment is measured in applied magnetic fields and no remanent magnetic moment exists. Paramagnetic minerals such as siderite or pyrite yield small but positive magnetic moment that quickly outweighs diamagnetic moments. Diamagnetism is a property of all matter and exhibits small and negative magnetic moments under an applied field (Dekkers 2007). Minerals such as quartz or calcite, dominant in cherts including those studied here, are diamagnetic (Evans and Heller 2003; Dunlop and Özdemir 1997). Diamagnetism is hundreds of times smaller than paramagnetism and thousands of times smaller than ferromagnetism (*s.l.*). For that reason, subtle variations in the

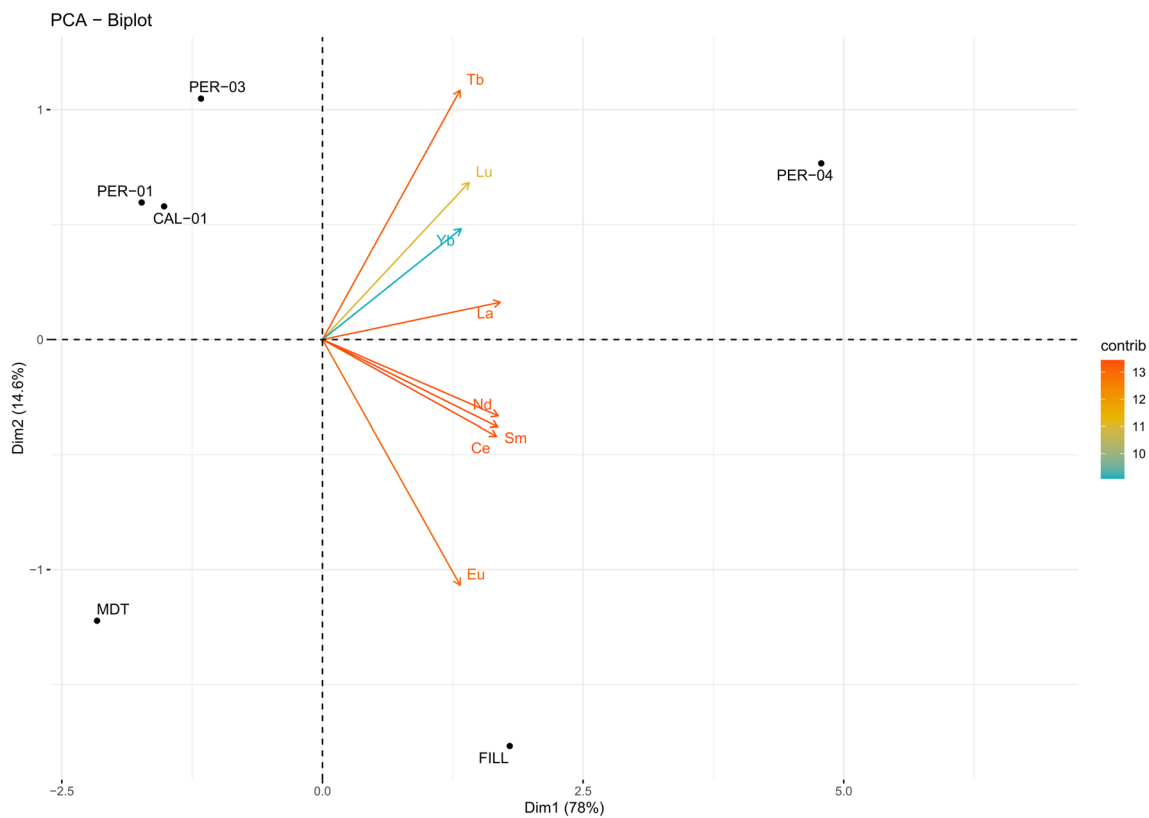


**Fig. 22** PCA NAA-REE

ferromagnetic mineralogy of these cherts dominate the magnetic signal and such differences in their magnetic properties can be interpreted in terms of different catchment areas, diagenesis, or subaerial exposition, for instance.

The results of the magnetic property analysis obtained here are consistent with similar works, highlighting in general the weak magnetization of cherts (e.g., Borradaile et al. 1998; Thacker & Ellwood 2002; Larrasoana et al. 2016; Ortega et al. 2018). However, among the geological samples studied, certain differences in the ferromagnetic mineral composition and concentration can be observed: magnetite is the dominant ferromagnetic mineral, but variable contributions of hematite are distinguished depending on the type of chert studied. A higher concentration of hematite is particularly visible in the FILL-01 and PER-04 chert types, whereas in the other cherts (CAL-01, MDT, PER-01, and PER-03), its contribution is very small or extremely difficult to distinguish by its magnetic properties alone. One of the main advantages of studying magnetic properties compared to other techniques is that instead of generically identifying iron (Fe) in the sample's composition, it allows detecting which specific ferromagnetic phase dominates the magnetization. This is the case of FILL-01 and PER-04 cherts where hematite was identified as the main iron oxide (Table 3 and Fig. 14),

whereas, broadly speaking, p-EDXRF or ICP-OES only detects the element (Fe) per se. It is also interesting that these two varieties of chert (FILL-01 and PER-04) are precisely the ones showing the highest concentration of iron in p-EDXRF and ICP-OES analyses (Tables 4 and 5, respectively). Basically, a good testimony of the complementarity of information that a multi-method comparative approach like this yield.

The homogeneous and high Fe values that grouped each two samples (FILL-01 and PER-04) are also consistent with the fieldwork data, as they are associated to gypsiferous and gray/red lutite lithofacies with a greater presence of oxide product of frequent subaerial exposures, and the results of thin-section (facies) analysis (see “[Petrographic analysis](#)”), p-EDXRF (see “[p-EDXRF](#)”) and ICP-OES (see “[ICP-OES](#)”).

The presence of Al detected for the FILL-01 and PER-04 samples by ICP-OES also confirms the occurrence of subaerial exposure episodes or post-genetic alterations, as Al is a major mineral component of exposure processes of gypsum and hydrated aluminum filosilicates conforming the enclosing rocks. When comparing the Mg–Al–Fe content (see Fig. 18a), the PER-01 and PER-03 cherts are separated from the rest, probably due to the deeper nature of its depositional environment and enclosing lithofacies

(gypsiferous marls and calcarenites lithofacies), suffering lesser exposure processes. The rest of the grouped chert types share shallow (gypsums) or marginal (lutites) enclosing lithofacies as depositional environments of the Paleogene saline lake that produced the Sant Genís Formation (Ortí et al. 2007). Comparing the Al-Ca-Fe content, the cherts are grouped (FILL-01 and PER-04) according to their measured Fe, a result which is also consistent with the results observed on the basis of ferromagnetic properties and confirmed by the other applied techniques, showing higher Fe content. PER-03 is also separated showing a higher content of Ca due to their calcareous origin and deepest stratigraphical position with no subaerial exposure processes.

Relative fractionations of rare-earth elements (REE) through NAA analyses have proved useful environmental indicators in chert of all geological ages, determining tectonic history and the sediment's depositional position within ocean basins from the relative contribution of end-member terrigenous (non-depleted in Ce) and seawater (Ce-depleted) sources (Murray 1994). In this work, REE analysis was applied to establish whether the so-called Ce-anomaly is valid for chert sources from inner platforms and continental environments. The results show that the Ce-anomaly in evaporitic cherts is always higher than 1 and the  $La_n/Ce_n$  ratio lower than 1, agreeing with the values from the continental margin environments noted by Murray (1994). Murray (1994) also pointed out that the presence of Ca, Mn, Mg, P, K, Na, Sr, Ba, Ge, Co, B, and V is in each case significantly affected by diagenetic processes and no longer reflects the depositional environment of the host sediment. PER-04 and FILL-01 are the only samples that present a major element marker with this technique, confirming also a higher Fe concentration (particularly hematite as shown by magnetic properties) (Table SII).

As mentioned in the results (“NAA”), and considering the geological data of the area (IGME 1975), the origin of the REE in cherts most probably is related to Triassic (Buntsandstein, Muschelkalk, and Keuper) and Paleozoic materials. These REE would be related to the different enclosing sediments and silicifications that have been incorporated throughout the time and diagenetic processes. The variability or similarities among samples likely depended on the composition of the older surrounding materials, as well as the sedimentary environment in which they were formed (Anadón et al. 1979; Gibbons & Moreno 2002).

As pointed out by Malyk-Selivanova et al. (1998) immobile elements detected by NAA analysis are excellent indicators of provenance and depositional environment because they can discriminate between different stratigraphic formations and units. As demonstrated, mobile elements, which can be detected using other techniques (such as EDXRF and ICP-OES), trace diagenetic environments by showing local

variations. Therefore, the identification of mobile element concentrations (such as Fe and Ca) contributes to differentiating chert varieties within a geological formation. In our study, the continental evaporitic depositional environments of the Sant Genís cherts forced us to consider mobile elements as markers of the diagenetic processes (Bustillo et al. 2012). Thus, the presence of Fe and/or Ca in samples may suggest differences among the enclosing lithological units and, as a result, distinctions in the particular chert outcrop.

### Consistency and challenges of the multi-technique approach

Three archaeological samples from the Abric Romaní site were chosen to assess the consistency/reliability of the geochemical analysis performed (Gómez de Soler et al. 2020a). Petrographically, these archaeological samples were assigned to various lithofacies from the analyzed formation: AR'02-M-U47-220 to PER-04; AR'02-M-P53-537 to CAL-01; and AR'01-M-Q47-49 to PER-01.

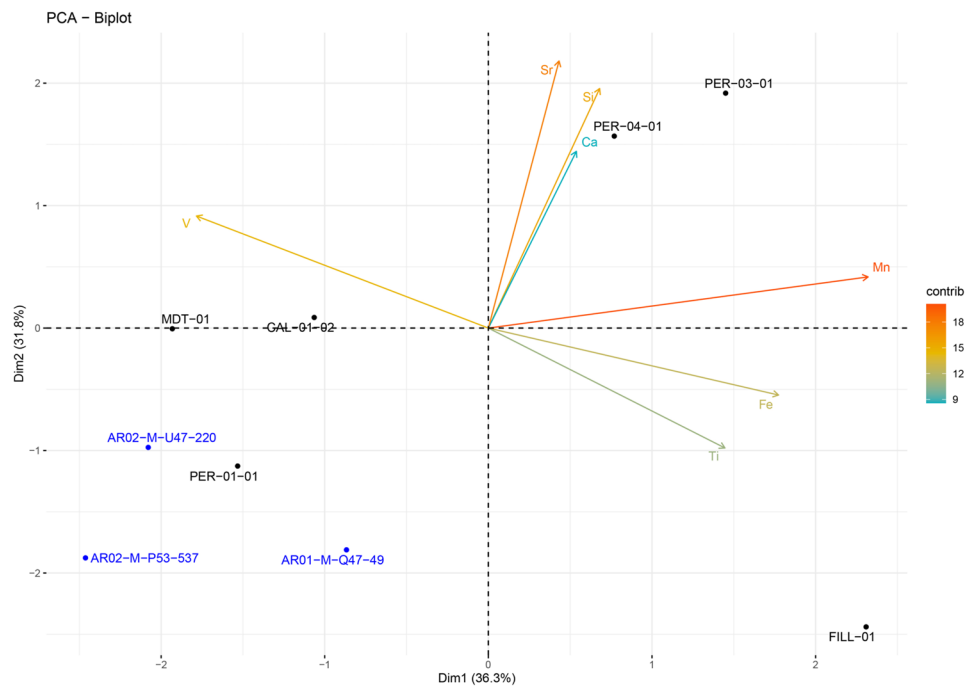
First, the Ce-anomaly obtained from these archaeological samples, as with the geological ones, shows a correlative ratio  $La_n/Ce_n$  where  $Ce_n/Ce_n^* > \sim 0.8$  and  $La_n/Ce_n < \sim 1$ , indicating similarities in their depositional environment (see Fig. 19).

XRD diffractograms indicate homogeneity among the geological and archaeological samples, with quartz as the main compositional phase, followed by moganite. However, variability in the results is detected by the p-EDXRF and in the content of trace elements and REE.

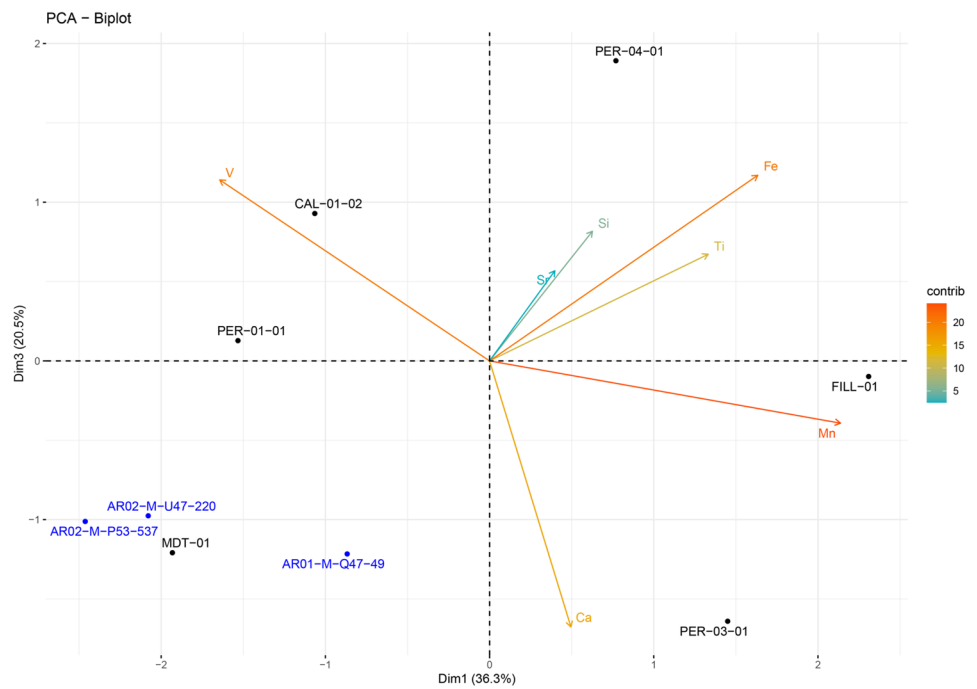
The PCA of the p-EDXRF (68.1% variance; components 1 and 2) (Fig. 23a) indicates similarities among the archaeological samples and the PER-01 chert type and MDT (56.8% variance; components 1 and 3) (Fig. 23b). The PCA of the NAA-REE results differs from the former petrographic ascriptions, suggesting the difficulty of ascribing early-diagenetic chert types to formations such as our study case, i.e., Cenozoic evaporites with so much vertical and lateral variability (Fig. 24). These results highlight the challenge of accurately differentiating chert varieties formed within similar physicochemical conditions using various analytical techniques, underscoring the need for larger sample sizes to encompass the full geochemical variability of chert. At this point, depending on the scale of analysis, it may be possible to ascribe the archaeological samples to the geological formation, but not to specific lithofacies of that formation. One point in favor is that the archaeological application to establish the catchment areas and the mobility routes that these communities had is not affected. All the outcrops are part of the same geological formation and are delimited in a specific area to the south of the municipality of Sant Martí de Tous, being considered varieties of the SMT chert type. However, this would not be valid if this siliceous



**Fig. 23** **a** PCA of the p-EDXRF of the geological and archaeological samples with 68.1% variance (components 1 and 2); **b** PCA of the geological and archaeological samples with 56.8% variance (components 1 and 3).



**a)**



**b)**

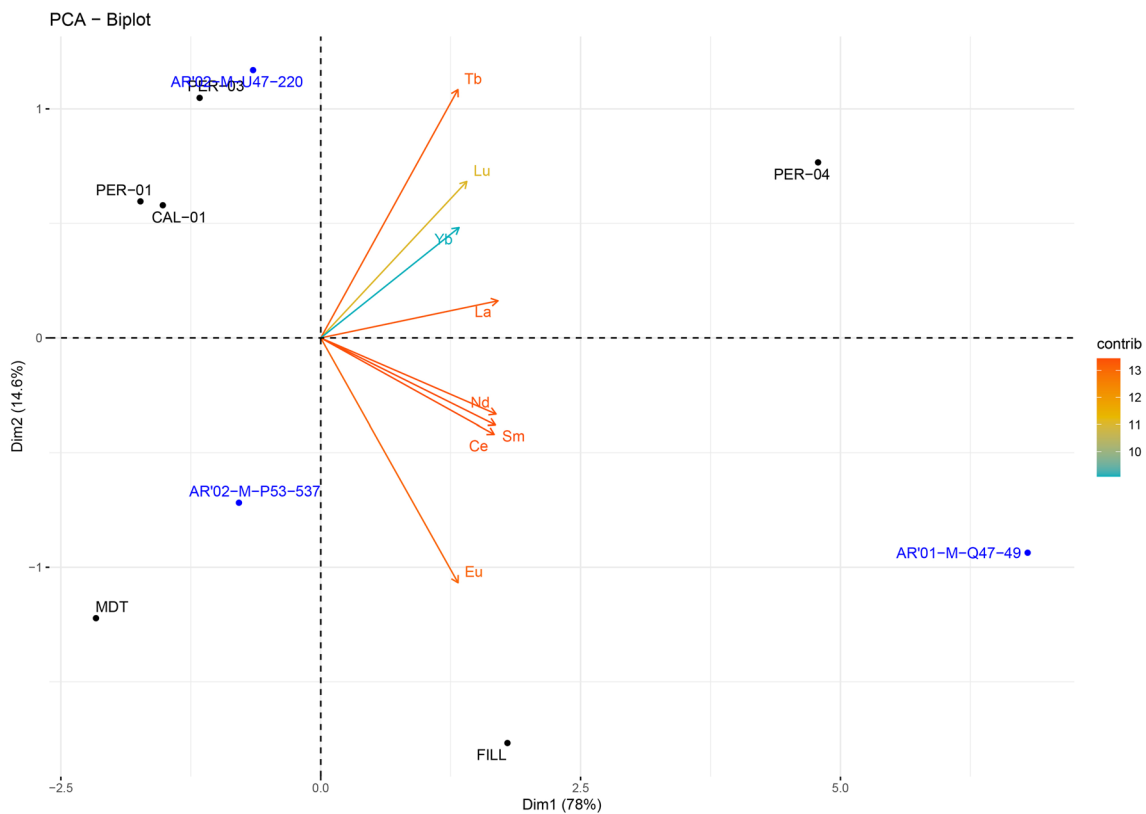


**Fig. 24** PCA of the NAA-REE of the geological and archaeological samples with 92.6% variance (components 1 and 2)

heterogeneity were to occur in a geological formation widely spread over a territory.

### Insights of the multi-technique approach

What are the most adequate current techniques for the characterization of Cenozoic evaporitic chert? XRD is an easy, accessible, and economical technique, but as it identifies crystalline phases, for cherts, it generally represents quartz as the predominant crystalline phase. The non-destructive version of this technique,  $\mu$ -XRD, only analyzes small surface areas (around  $1\text{mm}^2$ ) of the sample. This area can be increased by applying XY oscillation during the analysis. Magnetic property analysis is a fast and minimally invasive technique with more success in materials rich in ferromagnetic (*s.l.*) minerals like obsidian (Frahm et al. 2016), but it also has diagnostic potential for others lithologies including cherts (e.g., Larrasoana et al. 2016; Ortega et al. 2018). Even though cherts are diamagnetic rocks (do not preserve remanent magnetization), the analyses carried out in this study have successfully detected compositional and concentration differences in the Fe-bearing ferromagnetic mineralogy. Specifically, hematite has been identified and quantified as the most present iron oxide in FILL-01 and PER-04 chert varieties along with minor contributions of

magnetite also in the others. Identifying which specific ferromagnetic mineral is present is an information only provided in this study by the magnetic properties, regardless of other techniques that can also detect “iron” (broadly speaking). P-EDXRF has proved to be an excellent solution for characterization due to its non-destructive, accessible, and economical features (Gauthier et al. 2012; Roldán et al. 2015; Sánchez de la Torre et al. 2017b, 2020; Eixea et al. 2021, among others). ICP-OES is a useful technique, as has been demonstrated by other studies (Ramacciotti et al. 2019, 2022; Agam 2020). However, it is a destructive technology, and difficulties in the digestion processes call its suitability into question, especially when ICP-MS detects a greater number of different elements and does so more precisely (Navazo et al. 2008; Finkel et al. 2022, among others). Yet this has the same problems as ICP-OES, being a destructive technique with difficulties in the process of digestion. Laser ablation inductively coupled plasma mass spectrometry (LA-ICP-MS) might be a more appropriate technique, as various works have previously shown (Andreeva et al. 2014; Speer 2014; Gurova et al. 2016; Sánchez de la Torre et al. 2017a, 2020; Brandl et al. 2018; among others). NAA is a costly and destructive technique and not very versatile, as very few centers are equipped with the required facilities and technologies (Luedtke 1978; Malyk-Selivanova

et al. 1998; Huckell et al. 2011; Speer 2016; Prudêncio et al. 2016; Eixea et al. 2022, among others). Beyond the most commonly used techniques for rock characterization, there are other complementary techniques used in different works that have given good results and can be explored in the future. Examples are visible/near-infrared reflectance (VNIR) spectroscopy (Hubbard et al. 2004; Parish 2011, 2018), infrared reflectance microspectroscopy (IRRMS) (Hassler et al. 2013), Raman spectroscopy (Olivares et al. 2009; Capel Ferrón et al. 2015), trace element mapping with PIXE (Sánchez de la Torre et al. 2017a), and scanning electron microscopy with energy-dispersive X-ray spectroscopy (Abrunhosa et al. 2020).

Cenozoic evaporitic cherts are heterogeneous in nature, showing a high diversity of macroscopic, textural, geochemical, magnetic, and compositional traits that make it difficult to ascribe them precisely to different depositional environments and lithostratigraphic units (Colombo 1986; Ortí et al. 1997, 2007, 2014; Soto et al. 2014, 2023; Soto 2015; García-Simón & Domingo 2016; Gómez de Soler 2016; Gómez de Soler et al. 2020a). Facies analysis, systematic silicification samplings and samplings of enclosing rocks, and petrographic thin sections are shown to be traditional but appropriate techniques for differentiating chert varieties and different enclosing lithostratigraphic units.

Our analysis has shown that the individual application of modern compositional techniques may well fail to differentiate early-diagenetic cherts from a single geological formation, even from different lithological units. A combination of several techniques is to date the most adequate procedure for characterizing cherts and encompassing their variability. Exhaustive geoarchaeological prospections, facies recognition techniques, systematic sampling studies, macroscopic identification, petrographic thin-section analysis, and the application of several geochemical characterization techniques such as EDXRF and LC-ICP-MS would ensure proper characterization and geological ascriptions.

This study has highlighted the strengths and weaknesses of the different tests, evidencing the need for a variety of mineralogical and geochemical characterization techniques, as well as for a deep geological knowledge and exhaustive and systematic field recognition techniques to understand the full variability of prehistoric lithic raw materials. The differences and similarities shown by this study also bring to light the need for a systematic sampling of other regional formations yielding chert in order to establish a comparative framework. This would provide a starting point from which to consider the whole range of variability and the causes for the presence of the different trace elements and REE, allowing the different raw materials available to be quantitatively distinguished (Luedtke 1978; Malyk-Selivanova et al. 1998).

## Implications of the SMT chert in the archaeological assemblages

Due to its high concentration in a relatively small area (calculated using the CAR method) and its heterogeneity (in terms of size, shape, color, texture, and knappability), the SMT chert seems to have been a lithic resource that was long exploited by Pleistocene and early Holocene groups inhabiting an area ranging up to more than 50 km from the Sant Genís Formation. Archaeological examples of its exploitation are the Middle Paleolithic occupations of the Abric Romaní site (Gómez de Soler et al. 2020a), the Teixoneres cave with the evaporitic cherts documented there (currently under study), the many Mesolithic and Neolithic sites documented around the town of Sant Martí de Tous and along the Anoia Basin (Enrich 1981; Clop et al. 2005; Cámara 2017; Pujol 2016; Gómez de Soler et al. 2021), and the archaeological sites of the Cinglera del Capelló (e.g., Can Manel, Abric Agut) in Capellades (Vaquero et al. 2013) (15 km east of Sant Martí de Tous), attesting the continuous use of this chert type in the central part of the Catalan region (NE Iberian Peninsula).

This region is delimited by other areas with abundant chert sources. These include the Gaià and Francolí Basins, with the evaporitic cherts of the Valldeperes Formation (Lutetian) and the Bosc d'en Borrás Formation (Bartonian) (Gómez de Soler 2016), and the lacustrine cherts of the Castelltallat Formation in the Pre-Pyrenees (Roy et al. 2013; Sánchez de la Torre et al. 2017a, b; Ortega et al. 2018). To the northeast and east, a territory almost empty of chert is detected until beyond the Pyrenees in the Languedoc-Roussillon region (France). The only presence of chert, albeit scarce, is restricted to the Jurassic unit of the Illes Medes, the Cretaceous Montgrí Formation (Ortega et al. 2016), and the Neogene opaline formation of the Camp dels Ninots (Gómez de Soler et al. 2012) and Puig de les Molerers (Vehí 2001). In studies of lithic procurement in these regions, no chert from these formations has ever been documented (Ortega & Maroto 2001; Ortega 2002).

The near-absence of chert in the northeast and east of the NE Iberian Peninsula and the abundance and high quality of the SMT chert compared to other available lithologies justify the diachronic selection of SMT as a key chert source for central Catalonia. Further systematization of the mineralogical and geochemical characterization of the archaeological assemblages will enable SMT chert exploitation to be identified in prehistoric settlements.

## Conclusions

The SMT chert type is confirmed by its abundance at specific locations within a delimited territory in the NE Iberian Peninsula. The region is shown to be an important raw

material procurement area, as evidenced by the presence of the SMT chert type in the main prehistoric sites of the region (e.g., Abric Romaní, Cova de les Texioneres) and the constant discovery of new sites in the region around the Sant Genís Formation, especially from the Neolithic period onwards (e.g., Cal Sitjo, La Guinardera workshop, La Guinardera Nord workshop).

Through the characterization of cherts from the Sant Genís Formation, a Cenozoic evaporite formation, systematically sampled vertically and horizontally, this study confirms the great heterogeneity of Cenozoic cherts from the Sant Genís Formation (SMT chert type), widely exploited during the Pleistocene and Holocene of the Iberian Peninsula. This heterogeneity hampers the macroscopic characterization of the archaeological cherts, but petrographic analysis has enabled us to identify their origins and even, to a lesser extent, their lithostratigraphic unit of provenance within the formation. Complementary mineralogical and geochemical techniques applied in this study show that the application of specific criteria such as the concentration of Fe and Ca can assist in the identification of these cherts in one of the chert varieties of the SMT chert type, and consequently ascribe the procurement of these cherts to one of the outcrops of the Sant Genís Formation (SMT chert type).

As archaeologists, we are used to facing the sempiternal problem of correlating macroscopic and microscopic analytical scales, but the simultaneous use of multiple techniques can minimize the frequent inconsistencies of qualitative analysis. Intensive geoarchaeological survey programs, the identification of possible differences among the chert outcrops within a specific geological formation, exhaustive facies analysis, and sampling for reference collections, followed by macroscopic and petrographic thin-section characterization, combined with mineralogical and geochemical techniques, stand out as the ideal and most adequate practices for encompassing the variability of geological chert and thus for the correct and precise characterization of its provenance.

**Supplementary information** The online version contains supplementary material available at <https://doi.org/10.1007/s12520-023-01780-x>.

**Acknowledgements** We want to thank Debora Cano and Antonio de la Torre from the Servei de Recursos Científics i Tècnics of the Universitat Rovira i Virgili, who have helped us with the ICP-OES technology. Thanks to the Archaeonot-Research Project UAM. Thanks also to Rupert Glasgow for the English revision of the manuscript and to the anonymous reviewers for their comments and suggestions that have improved the manuscript.

**Author contribution** B. G. S.: conceptualization; methodology; writing—original draft; investigation. M. S.: methodology; investigation; writing—review and editing. A. C.: magnetic property analysis, investigation, and data curation. F. G. G.: X-ray diffraction, investigation, and data curation. H. M.: neutron activation analysis, investigation,

and data curation. C. R. and A. E.: portable energy-dispersive X-ray fluorescence analysis, investigation, and data curation. A. M. P., M. G. Ch., M. S. R., and J. V.: investigation and data curation. All authors reviewed the manuscript.

**Funding** Open access funding provided by Universitat Rovira i Virgili. Funding for this research was provided by the Departament de Cultura of the Generalitat de Catalunya project no. CLT009/22/000044, the Catalan Government research group nos. 2021 SGR 01238 and 2021 SGR 01237, and by the Spanish Government project PID2019-103987 GB-C31 and PID2021-123092NB-C21. The research of B. G. S., M. G. Ch., and J. V. is funded by the CERCA Programme/Generalitat de Catalunya. The research of M. S. is funded by the UAM-2019 Tomás y Valiente Program. The research of A. C. is funded by the project PID2019-105796 GB-I00 of the Agencia Estatal de Investigación (AEI/<https://doi.org/10.13039/501100011033>). M. S. R. is funded by a PTA contract (PTA2018-016561-I). The research of A. M. is supported by the Reclassification of the University System, Margarita Salas modality. The research of A. E. was supported by the 2018 Leonardo Project for Researchers and Cultural Creators (BBVA Foundation), GV/2021/054 project from Generalitat Valenciana, and PID2021-122308NA-I00 project from the Agencia Estatal de Investigación. The Institut Català de Paleoeologia Humana i Evolució Social (IPHES-CERCA) has received financial support from the Spanish Ministry of Science and Innovation through the “María de Maeztu” program for Units of Excellence (CEX2019-000945-M).

**Data availability** All data generated or analyzed during this study are included in this published article (and its supplementary information files).

**Code availability** Not applicable.

## Declarations

**Ethics approval** Not applicable.

**Consent to participate** All authors consent to the participation.

**Consent for publication** All authors consent to the publication.

**Competing interests** The authors declare no competing interests.

**Open Access** This article is licensed under a Creative Commons Attribution 4.0 International License, which permits use, sharing, adaptation, distribution and reproduction in any medium or format, as long as you give appropriate credit to the original author(s) and the source, provide a link to the Creative Commons licence, and indicate if changes were made. The images or other third party material in this article are included in the article's Creative Commons licence, unless indicated otherwise in a credit line to the material. If material is not included in the article's Creative Commons licence and your intended use is not permitted by statutory regulation or exceeds the permitted use, you will need to obtain permission directly from the copyright holder. To view a copy of this licence, visit <http://creativecommons.org/licenses/by/4.0/>.

## References

- Abrunhosa A, Bustillo MÁ, Pereira T, Márquez B, Pérez-González A, Arsuaga JL, Baquedano E (2020) Petrographic and SEM-EDX characterization of Mousterian white/beige chert tools from the Navalmaíllo rock shelter (Madrid, Spain). *Geoarchaeology* 35(6):883–896. <https://doi.org/10.1002/gea.21811>

- Agam A (2020) Late lower paleolithic lithic procurement and exploitation strategies: a view from Acheulo-Yabrudian Qesem Cave (Israel). *J Archaeol Sci Rep* 33:102447. <https://doi.org/10.1016/j.jasrep.2020.102447>
- Anadón P, Colombo F, Esteban M, Marzo M, Robles S (1979) Evolución tectonoestratigráfica de los Catalánides. *Acta Geologica Hispanica* 14(1):242–270
- Anadón P, Cabrera L, Colldeforns B, Sáez A (1989) Los sistemas lacustres del Eoceno superior y Oligoceno del sector oriental de la Cuenca del Ebro. *Acta Geológica Hispánica* 24(3–4):205–230
- Andreeva P, Stefanova E, Gurova M (2014) Chert raw materials and artefacts from NE Bulgaria: a combined petrographic and LA-ICP-MS study. *J Lithic Stud* 1(2):25–45. <https://doi.org/10.2218/jls.v1i2.1129>
- Bloemendal J, King JW, Hall FR, Doh SJ (1992) Rock magnetism of Late Neogene and Pleistocene deep-sea sediments: relationship to sediment source, diagenetic processes and sediment lithology. *J Geophys Res* 97(B4):4361–4375
- Borradaile GJ, Stewart JD, Ross WA (1998) Characterizing stone tools by rock-magnetic methods. *Geoarchaeology* 13(1):73–91. [https://doi.org/10.1002/\(SICI\)1520-6548\(199801\)13:1%3c73::AID-GEA5%3e3.0.CO;2-5](https://doi.org/10.1002/(SICI)1520-6548(199801)13:1%3c73::AID-GEA5%3e3.0.CO;2-5)
- Brandl M, Martinez MM, Hauzenberger C, Filzmoser P, Nymoen P, Mehler N (2018) A multi-technique analytical approach to sourcing Scandinavian flint: provenance of ballast flint from the shipwreck “Leirvigen 1”, Norway. *PLoS ONE* 13(8):e0200647. <https://doi.org/10.1371/journal.pone.0200647>
- Bruker-AXS (2009) General profile and structure analysis software for powder diffraction data.
- Bustillo MÁ, Pérez-Jiménez JL, Bustillo M (2012) Caracterización geoquímica de rocas sedimentarias formadas por silicificación como fuentes de suministro de utensilios líticos (Mioceno, cuenca de Madrid). *Revista Mexicana De Ciencias Geológicas* 29(1):233–247
- Cámara J (2017) L’exploració de roques silícies procedents de Tous al llarg de la prehistòria. Estat de la qüestió sobre les recerques arqueològiques desenvolupades fins a l’actualitat. *Miscellanea Aqualatensis* 17:47–63
- Capel Ferrón C, León-Reina L, Jorge-Villar S, Compañía JM, Aranda MAG, López Navarrete JT, Hernández V, Medianero FJ, Ramos J, Weniger GC, Domínguez-Bella S, Linstaedter J, Cantalejo P, Espejo M, Valsero JJD (2015) Combined Raman spectroscopic and Rietveld analyses as a useful and nondestructive approach to studying flint raw materials at prehistoric archaeological sites. *Archaeol Anthropol Sci* 7(2):235–243. <https://doi.org/10.1007/s12520-014-0189-0>
- Cheary R, Coelho A, Cline J (2004) Fundamental parameters line profile fitting in laboratory diffractometers. *J Res Natl Inst of Stand Technol* 109:1–25
- Chowns TM, Elkins JE (1974) The origin of quartz geodes and cauliflower cherts through the silicification of anhydrite nodules. *J Sediment Petrol* 44(3):885–903
- Clop X, Faura JM, Piqué R, Gibaja JF (2005) Els Vilars de Tous (Igualada, Barcelona): una estructura de habitació i producció lítica del V mil·lenni cal BC. I. In R. Roberto Ontañón, C. García-Moncó, & P. Arias (Eds.). *Actas del III Congreso del Neolítico en la Península Ibérica*. Universidad de Cantabria. Santander, pp. 551–558.
- Colldeforns B, Anadón P, Cabrera L (1994) Litoestratigrafía del Eoceno superior-Oligoceno inferior de la zona oriental de la Cuenca del Ebro. Sector Igualada-Santa Coloma De Queralt *Geogaceta* 15:55–58
- Colombo F (1986) Estratigrafía y sedimentología del Paleogeno continental del borde meridional occidental de los Catalanides (Provincia de Tarragona, España). *Cuadernos Geología Ibérica* 10:55–115
- Day R, Fuller M, Schmidt VA (1977) Hysteresis properties of titanomagnetites: Grain size and composition dependence. *Phys Earth Planet Inter* 13:260–267
- Dekkers MJ (2007) Magnetic proxy parameters. In: Gubbins D, Herrero-Bervera E (eds) *Encyclopedia of Geomagnetism and Palaeomagnetism*. Springer, pp 525–534
- Dollase W (1986) Correction of intensities for preferred orientation in powder diffractometry: application of the March model. *J Appl Crystallogr* 19:267–272
- Dunlop DJ, Özdemir Ö (1997) *Rock magnetism: fundamentals and frontiers*. Cambridge Univ. Press, New York, p 573
- Edo M, Antolín F, Barrio MJ (2012) Can Sadurní (Begues, Baix Llobregat), de la captació de recursos abiòtics al inici de la mineria de alumino-fosfats (10 500–4000 cal. a. n. e.) en el Macizo de Garraf. *Rubricatum* 5:299–306
- Eixea A, Martínez-Alfaro A, Bel MA, Roldán C, Murcia S, Vie D, Sanchis A, Villaverde V (2021) First data on the characterization of siliceous raw materials and catchment areas from Cova de les Malladetes (Valencia, Spain). In G Lengyel, J Wilczyński, M Sánchez de la Torre, X Mangad & JM Fullola (Eds.), *Studies on the Palaeolithic of Western Eurasia*. Archaeopress publishing pp. 205–215.
- Eixea A, Roldán C, Villaverde V, Dias MI, Prudêncio MI, Marques R, Russo D, Gmélíng K, Cavallo G, Murcia S (2022) Geochemical and petrographic analyses on Middle and Upper Palaeolithic cherts from the central region of Mediterranean Iberia. *Lithic Technol*. <https://doi.org/10.1080/01977261.2022.2097811>
- Enrich J (1981) Estació-Taller de sílex a Sant Pere de l’Erm (Sant Martí de Tous, Anoia). In A. de S. M. de Tous (Ed.) *Tous, Mil anys d’Història*. Publicacions de l’Abadia de Montserrat, pp. 9–22.
- Estévez J, Piqué R, Weniger G-C, Bonet A, Clemente-Conte I (1993) El poblamiento Prehistórico en la cuenca del Mediona (Alt Penedès, Barcelona). *Trabalhos De Antropologia e Etnologia* 2:119–136
- Evans ME, Heller F (2003) *Environmental magnetism: principles and applications of environmagnetics*. Academic Press, San Diego, CA, p 299
- Finkel M, Erel Y, Ben Dor Y, Tirosh O, Levy TE, Najjar M, Avni Y, Gopher A, Ben-Yosef E (2022) High resolution elemental characterization of prehistoric flint sources in southern Israel: implications for archaeological provenance studies. *J Archaeol Sci Rep* 43:103438. <https://doi.org/10.1016/j.jasrep.2022.103438>
- Frahm E, Feinberg JM, Monnier GF, Tostevin GB, Gasparyan B, Adler DS (2016) Lithic raw material units based on magnetic properties: a blind test with Armenian obsidian and application to the Middle Palaeolithic site of Lusakert Cave 1. *J Archaeol Sci* 74:102–123. <https://doi.org/10.1016/j.jas.2016.09.001>
- Freixas A, Mir A (1987) El jaciment paleolític de la Noguera a Sant Quintí de Mediona, Alt Penedès. *Cypsela* VI: 191–200.
- Fullola JM, Bartolí R, Cebrià A, Bergadà MM, Farell D, Nadal J (2020) El Paleolítico Superior de Catalunya: el Gravetiense de la Balma de la Griera (Calafell, Baix Penedès, Tarragona). *Trabalhos de Antropologia e Etnologia* 34(1–2): 35–52.2
- García-Simón LM, Domingo R (2016) The Monegros-type chert: petrographic characterization and prehistoric use. *J Lithic Stud* 3(2):357–374. <https://doi.org/10.2218/jls.v3i2.1417>
- Gauthier G, Burke AL, Leclerc M (2012) Assessing XRF for the geochemical characterization of radiolarian chert artifacts from northeastern North America. *J Archaeol Sci* 39(7):2436–2451. <https://doi.org/10.1016/j.jas.2012.02.019>
- Gibbons W, Moreno T (2002) The geology of Spain. *Geological Society of London*. <https://doi.org/10.1144/GOSPP>
- Gómez de Soler B, Campeny Vall-Llosera G, van der Made J, Oms O, Agustí J, Sala R, Blain HA, Burjachs F, Claude J, García Catalán S, Riba D, Rosillo R (2012) A new key locality for the Pliocene vertebrate record of Europe: the Camp dels Ninots maar

- (NE Spain). *Geol Acta* 10(1):1–17. <https://doi.org/10.1344/105.00001702>
- Gómez de Soler B (2016) Procedencia del aprovisionamiento lítico durante el Paleolítico medio en el yacimiento del Abric Romaní (Capellades, Barcelona). Niveles M, Oa y P. Dissertation, Universitat Rovira i Virgili.
- Gómez de Soler B, Chacón MG, Bargalló A, Romagnoli F, Soto M, Vallverdú J, Vaquero M (2019) Mobilité territoriale pendant le Paléolithique moyen en contextes discoïde et Levallois : exemple du site de l’Abric Romaní (Capellades, Barcelona, Espagne), niveau M et sous-niveau Oa. *La Conquête de La Montagne : Des Premières Occupations Humaines à l’anthropisation Du Milieu*. <https://doi.org/10.4000/books.cths.6212>
- Gómez de Soler B, Soto M, Vallverdú J, Vaquero M, Bargalló A, Chacón MG, Romagnoli F, Carbonell E (2020) Neanderthal lithic procurement and mobility patterns through a multi-level study in the Abric Romaní site (Capellades, Spain). *Quat Sci Rev* 237:106315. <https://doi.org/10.1016/j.quascirev.2020.106315>
- Gómez de Soler B, Soto M, Vallverdú J, Bargalló A, Chacón MG, Romagnoli F, Vaquero M (2020b) The Panadella chert (Montmaneu Formation): a high-quality raw material in the Abric Romaní sequence (NE Iberian Peninsula). *Archaeol Anthropol Sci* 12(11). <https://doi.org/10.1007/s12520-020-01198-9>
- Gómez de Soler B, Soares-Remiseiro M, Arteaga-Brieba A, Borràs G, Cámara J, Campeny G, Chacón MG, Fernández-Marchena JL, Guinart V, López G, Mas B, Soto M, Suesta A, Shkarinska K, Ramírez-Pedraza I, Val-Peón C, Vallverdú J (2021) The Guinardera quarry (Sant Martí de Tous, Barcelona): a new chert exploitation location during historical times. *J Lithic Stud* 8(2):1–24. <https://doi.org/10.2218/jls.6546>
- Graetsch HA, Grünberg JM (2012) Microstructure of flint and other chert raw materials. *Archaeometry* 54(1):18–36. <https://doi.org/10.1111/j.1475-4754.2011.00610.x>
- Grommé CS, Wright TL, Peck D (1969) Magnetic properties and oxidation of iron-titanium oxide minerals in Alae and Makaopuhi lava lakes. *Hawaii J Geophys Res* 74:5277–5294
- Gurova M, Andreeva P, Stefanova E, Stefanov Y, Kočić M, Borić D (2016) Flint raw material transfers in the prehistoric Lower Danube Basin: an integrated analytical approach. *J Archaeol Sci Rep* 5:422–441. <https://doi.org/10.1016/j.jasrep.2015.12.014>
- Hamilton NE, Ferry M (2018) Ggtern: ternary diagrams using ggplot2. *J Stat Softw Code Snippets* 87(3):1–17
- Hassler ER, Swihart GH, Dye DH, Li YS (2013) Non-destructive provenance study of chert using infrared reflectance microspectroscopy. *J Archaeol Sci* 40(4):2001–2006. <https://doi.org/10.1016/j.jas.2012.12.028>
- Hubbard MJ, Waugh DA, Ortiz JD (2004) Provenance determination of archaeological cherts by Vis/NIR diffuse reflectance spectrometry. *The Compass* 78(3):119–129
- Huckell BB, Kilby JD, Boulanger MT, Glascock MD (2011) Sentinel Butte: neutron activation analysis of White River Group chert from a primary source and artifacts from a Clovis cache in North Dakota, USA. *J. Archaeol. Sci.* 38: 965–976. <https://doi.org/10.1016/j.jas.2010.11.011>
- IGME (1975) Mapa Geológico de España. Escala 1:50.000. Hoja n°391 (Igualeda). Serie Magna. IGME, Madrid
- Kassambara A, Mundt F (2017) Factoextra: extract and visualize the results of multivariate data analyses. R-package version 1.0.7. <https://cran.r-project.org/package=factoextra>
- Knauth LP (1994) Petrogenesis of Chert *Rev Mineral Geochem* 29:233–258
- Kruiver PP, Passier HF (2011) Coercivity analysis of magnetic phases in sapropel S1 related to variations in redox conditions, including an investigation of the S ratio. *Geochem Geophys Geosyst* 2:1–21. <https://doi.org/10.1029/2001GC000181>
- Larrasoña JC, Beamud E, Olivares M, Murelaga X, Tarrío A, Baceta JJ, Etxebarria N (2016) Magnetic properties of cherts from the Basque-Cantabrian Basin and surrounding regions: archaeological implications. *Frontiers in Earth Sci* 4. <https://doi.org/10.3389/feart.2016.00035>.
- Le S, Josse J, Husson F (2008) FactoMineR: an R package for Multivariate Analysis. *J Stat Softw* 25(1):1–18
- Leonhardt R (2006) Analyzing rock magnetic measurements: the RockMagAnalyzer 1.0 software. *Computers and Geosciences* 32(9):1420–1431
- Luedtke BE (1978) Chert sources and trace-element analysis. *Am Antiq* 43(3):413–423. <https://doi.org/10.2307/279398>
- Malyk-Selivanova N, Ashley GM, Gal R, Glascock MD, Neff H (1998) Geological–geochemical approach to “sourcing” of prehistoric chert artifacts, northwestern Alaska. *Geoarchaeology* 13(7):673–708. [https://doi.org/10.1002/\(SICI\)1520-6548\(199810\)13:7%3c673::AID-GEA2%3e3.0.CO;2-3](https://doi.org/10.1002/(SICI)1520-6548(199810)13:7%3c673::AID-GEA2%3e3.0.CO;2-3)
- Mommsen H, Kreuser A, Lewandowski E, Weber J (1991) Provenancing of pottery: a status report on neutron activation analysis and classification. In M. Hughes, C. M., & D. Hook (Eds.), *Neutron Activation and Plasma Emission Spectrometric Analysis in Archaeology*. British Museum, pp. 57–65.
- Morales JJ, Cebrià A, Burguet-Coca A, García-Argudo G, Rodríguez-Hidalgo A, Soto M, Talamo S, Tejero JM, Vallverdú J, Fullola JM (2019) The Middle-to-Upper Paleolithic transition occupations from Cova Foradada (Calafell, NE Iberia). *PLoS ONE* 14(5):e0215832
- Morales JJ, Cebrià A, Vergès JM, Bañuls-Cardona S, Cervelló JM, Hernando R, Lombao D, Marín J, Marsal R, Oms FX, Rabuñal J, Rodríguez-Hidalgo A, Soto M, Rosas A, Fullola J (2022) Palaeolithic archaeology in the conglomerate caves of north-eastern Iberia. *Antiq Project Ga*. <https://doi.org/10.15184/aqy.2022.34>
- Munsell Color (2013) Munsell Rock Color Book. Geological Society of America (GSA), Grand Rapids (Michigan), 19 p.
- Murray RW (1994) Chemical-criteria to identify the depositional environment of chert - general-principles and applications. *Sediment Geol* 90(93):213–232
- Murray RW, Tenbrink MRB, Jones DL, Gerlach DC, Russ GP (1990) Rare-earth elements as indicators of different marine depositional-environments in chert and shale. *Geol* 18(3):268–271. [https://doi.org/10.1130/0091-7613\(1990\)018%3c0268:Reeai0%3e2.3.Co;2](https://doi.org/10.1130/0091-7613(1990)018%3c0268:Reeai0%3e2.3.Co;2)
- Navazo M, Colina A, Domínguez-Bella S, Benito-Calvo A (2008) Raw stone material supply for Upper Pleistocene settlements in Sierra de Atapuerca (Burgos, Spain): flint characterization using petrographic and geochemical techniques. *J Archaeol Sci* 35(7):1961–1973. <https://doi.org/10.1016/j.jas.2007.12.009>
- Olivares M, Tarrío A, Murelaga X, Baceta JJ, Castro K, Etxebarria N (2009) Non-destructive spectrometry methods to study the distribution of archaeological and geological chert samples. *Spectrochimica Acta - Part a: Molecular and Biomolecular Spectroscopy* 73(3):492–497. <https://doi.org/10.1016/j.saa.2008.12.036>
- Oms FX, Mestres J, Cebrià A, Morales JJ, Nadal J, Pedro M, Mendiola S, Martín P, Fullola JM (2016) La cova de la Guineu (Font-rubí, Barcelona) I les relacions plana-muntanya al Penedès durnat el neolític inicial. *Del Neolític a l’Edat de Bronze En El Mediterrani Occidental. Serie De Trabajos Varios* 119:97–108
- Oms FX, Mestres J, Martínez-Grau H, Laborda R, Antolín F, Bergadà MM, Emens A, Gibaja JJ, González Olivares C, Mangado X, Martín P, Mas B, Nadal J, Fullola JM (2021) Fases de ocupación y estratigrafía del asentamiento neolítico de Les Guixeres de Vilobí (Sant Martí Sarroca, Barcelona). *Trabajos De Prehistoria* 78(2):257–276. <https://doi.org/10.3989/tp.2021.12275>
- Ortega D (2002) Mobilitat i desplaçaments dels grups caçadors-recol·lectors a inicis del paleolític Superior a la regió Pirinenca Oriental. *Cypsel* 14:11–26

- Ortega D, Maroto J (2001) Matières premières et technologie lithique du Moustérien final de la grotte des Ermitons (Pyrénées Méditerranéennes). *Les Premiers Hommes Modernes de La Péninsule Ibérique. Actes Du Colloque de La Commission VIII de l'UISPP*, pp. 69–76.
- Ortega D, Roqué C, Terradas X (2016) Disponibilidad De Rocas Silíceas En El Noreste Peninsular. *CPAG* 26:245–282
- Ortega D, Roqué C, Ibáñez J, Beamud E, Larrasoña JC, Sáez A, Terradas X (2018) The chert from the Castellallat Formation (south-central Pyrenees): archaeometric characterisation and archaeological implications. *Archaeol Anthropol Sci* 10:1329–1346. <https://doi.org/10.1007/s12520-016-0458-1>
- Ortí F, Rosell L, Salvany JM, Inglès M (1997) Chert in continental evaporites of the Ebro and Calatayud Basins (Spain): distribution and significance. In: A Ramos-Millán, A & MA Bustillo (Eds.). *Siliceous Rocks and Culture. Universidad de Granada, Monográfica Arte y Arqueología* 42: 75–89.
- Ortí F, Rosell L, Inglès M, Playà E (2007) Depositional models of lacustrine evaporites in the SE margin of the Ebro Basin (Paleogene, NE Spain). *Geol Acta* 5(1):19–34
- Ortí F, Rosell L, Gibert L, Moragas M, Playà E, Inglès M, Rouchy JM, Calvo JP, Gimeno D (2014) Evaporite sedimentation in a tectonically active basin: the lacustrine Las Minas Gypsum unit (Late Tortonian, SE Spain). *Sediment Geology* 311:17–42. <https://doi.org/10.1016/j.sedgeo.2014.06.004>
- Parish RM (2011) The application of visible/near-infrared reflectance (VNIR) spectroscopy to chert: a case study from the Dover Quarry sites. *Tennessee Geoarchaeology* 26(3):420–439. <https://doi.org/10.1002/gea.20354>
- Parish RM (2018) Lithic procurement patterning as a proxy for identifying Late Paleoinidian group mobility along the Lower Tennessee River Valley. *J Archaeol Sci Rep* 22:313–323. <https://doi.org/10.1016/j.jasrep.2016.03.028>
- Picin A, Chacón MG, Gómez de Soler B, Blasco R, Rivals F, Rosell J (2020) Neanderthal mobile toolkit in short-term occupations at Teixoneres Cave (Moia, Spain). *J. Archaeol Sci Rep* 29:102165. <https://doi.org/10.1016/j.jasrep.2019.102165>
- Piper DZ, Bau M (2013) Normalized rare earth elements in water, sediments, and wine: identifying sources and environmental redox conditions. *Am J Analytical Chem* 4:69–83
- Pujol A (2016) Sant Martí de Tous. Revisió de l'inventari del poblament des de la Prehistòria fins a l'Edat Mitjana. Ed. Diputació de Barcelona, Sant Martí de Tous, 52 p.
- Prudêncio MI, Roldán C, Dias MI, Marques R, Eixea A, Villaverde V (2016) A micro-invasive approach using INAA for new insights into Palaeolithic flint archaeological artefacts. *J Radioanalytical Nucl Chem* 308(1):195–203. <https://doi.org/10.1007/s10967-015-4294-z>
- Ramacciotti M, Gallello G, Pastor A, Diez-Castillo A, Or G-P (2019) Chert nucleus and cortex characterization for archaeological provenance study tested in the Prebaetic System Region (Valencian Community, Spain). *Lithic Technol* 44(3):166–180. <https://doi.org/10.1080/01977261.2019.1618043>
- Ramacciotti M, García-Puchol O, Cortell-Nicolau A, Gallello G, Morales-Rubio A, Pastor A (2022) Moving to the land: first archaeometric study of chert procurement at Cueva de la Cocina (Eastern Iberia). *Geoarchaeology* 37:544–559. <https://doi.org/10.1002/gea.21903>
- Rey-Solé M, Mangado J, Daura J, Sanz M (2014) Caracterización de las materias primas líticas del yacimiento paleolítico de la Dolina de l'Esquerda de les Alzines (macizo del Garraf, Barcelona). *Pyrenae* 45(1):31–54. <https://doi.org/10.1344/Pyrenae2014.vol45num1.2>
- Rietveld H (1969) A profile refinement method for nuclear and magnetic structures. *J Appl Cryst* 2:65–71
- Roberts AP, Cui Y, Verosub KL (1995) Wasp-waisted hysteresis loops: mineral magnetic characteristics and discrimination of components in mixed magnetic systems. *J Geophysical Res. Soil Earth* 100(B9):17909–17924. <https://doi.org/10.1029/95JB00672>
- Roldán C, Carballo J, Murcia S, Eixea A, Villaverde V, Zilhão J (2015) Identification of local and allochthonous flint artefacts from the Middle Palaeolithic site “Abrigo de la Quebrada” (Chelva, Valencia, Spain) by macroscopic and physicochemical methods. *X-Ray Spectrom* 44(4):209–216. <https://doi.org/10.1002/xrs.2602>
- Roy M, Tarriño A, Benito-Calvo A, Mora R, Martínez-Moreno J (2013) Aprovechamiento de sílex en el Prepirineo oriental durante el Paleolítico superior antiguo: El nivel arqueológico 497C de Cova Gran (Santa Linya, Lleida). *Trab Prehist* 70(1):7–27. <https://doi.org/10.3989/tp.2013.12100>
- Saez A (1987). *Estratigrafía y sedimentología de las formaciones lacustres del tránsito Eoceno-Oligoceno del NE de la cuenca del Ebro*. Dissertation, Universitat de Barcelona.
- Sánchez de la Torre M, Angyal A, Kertész Z, Dubernet S, Le Bourdonnec FX, Csedreki L, Furu E, Papp E, Szoboszlai Z, Szikszai Z (2017a) Trace element mapping of two Pyrenean chert deposits (SW Europe) by PIXE. *Nucl Instrum Methods Phys Res, Sect B* 400:58–64. <https://doi.org/10.1016/j.nimb.2017.04.016>
- Sánchez de la Torre M, Le Bourdonnec FX, Gratuze B, Domingo R, García-Simón LM, Montes L, Mazo C, Utrilla P (2017b) Applying ED-XRF and LA-ICP-MS to geochemically characterize chert. The case of the Central-Eastern Pre-Pyrenean lacustrine cherts and their presence in the Magdalenian of NE Iberia. *J Archaeol Sci Rep* 13:88–98. <https://doi.org/10.1016/j.jasrep.2017.03.037>
- Sánchez de la Torre M, Utrilla P, Domingo R, Jiménez L, Le Bourdonnec FX, Gratuze B (2020) Lithic raw material procurement at the Chaves cave (Huesca, Spain): a geochemical approach to defining Palaeolithic human mobility. *Geoarchaeology* 35(6):856–870. <https://doi.org/10.1002/gea.21808>
- Solé Sabarís L (1964) *Geografía de Catalunya*. Aedos.
- Solé VA, Papillon E, Cotte M, Walter P, Susini J (2007) A multiplatform code for the analysis of energy-dispersive X-ray fluorescence spectra. *Spectrochimica Acta Part B: Atomic Spectroscopy* 61(1):63–68. <https://doi.org/10.1016/j.sab.2006.12.002>
- Soto M (2015) *Áreas y estrategias de aprovisionamiento lítico de los últimos cazadores-recolectores en las montañas de Prades (Tarragona)*. Dissertation, Universitat Rovira i Virgili.
- Soto M, Gómez de Soler B, Vallverdú J, Vaquero M (2014) Potential siliceous sources during Prehistory: results of prospecting in the East margin of the Ebro Basin (NE Iberian Peninsula). *J Lithic Stud* 1(1):293–318. <https://doi.org/10.2218/jls.v1i1.772>
- Soto M, Gómez de Soler B, Vallverdú J (2018) The chert abundance ratio (CAR): a new parameter for interpreting Palaeolithic raw material procurement. *Archaeol Anthropol Sci* 10(8):2027–2046. <https://doi.org/10.1007/s12520-017-0516-3>
- Soto M, Chacón MG, Aourache H, Morales JI, Haddoumi H, Souhir M, Benito-Calvo A, Tarriño A, Bengamra S, Salazar-Ramos R (2023) Raw material procurement and territorial mobility in the Aïn Beni Mathar-Guefaït Region (Eastern

- Morocco). In: C. Speers, R.M., Parish, G. Barrientos (Eds.) Sourcing Lithic Archaeological Assemblages, University of Utha, pp. 121–131.
- Speer ChA (2014) LA-ICP-MS analysis of Clovis period projectile points from the Gault Site. *J Archeol Sci* 52:1–11. <https://doi.org/10.1016/j.jas.2014.08.014>
- Speer ChA (2016) A comparison of instrumental techniques at differentiating outcrops of Edwards Plateau chert at the local scale. *J Archaeol Sci Rep* 7:389–393. <https://doi.org/10.1016/j.jasrep.2016.05.026>
- Team RC (2021) R: a language and environment for statistical computing. R Foundation for Statistical Computing.
- Thacker PT, Ellwood BB (2002) The magnetic susceptibility of cherts: archaeological and geochemical implications of source variation. *Geoarchaeology* 17(5):465–482. <https://doi.org/10.1002/gea.10023>
- Vaquero M, Allué E, Alonso S, Bischoff JL, Burjachs F, Vallverdú J (2006) El Abric Agut (Capellades, Barcelona) y el Mesolítico de muescas y denticulados en el noreste de la Península. In N. Bicho & H. Verissimo (Eds.) *Do Epipaleolítico na Península Ibérica*. Universidade do Algarve, pp. 113–122.
- Vaquero M, Allué E, Bischoff JL, Burjachs F, Vallverdú J (2013) Environmental, depositional and cultural changes in the Upper Pleistocene and Early Holocene: the Cinglera del Capelló sequence (Capellades, Spain). *Quaternaire* 24(1):49–64
- Vehí M (2001) Geologia ambiental de la depressió de la Selva. Dissertation, Universitat Autònoma de Barcelona.
- Wickham H (2016). *ggplot2: elegant graphics for data analysis*. Springer-Verlag New York.

**Publisher's note** Springer Nature remains neutral with regard to jurisdictional claims in published maps and institutional affiliations.